

RESEARCH ARTICLE

Open Access



Single molecule array measures of LRRK2 kinase activity in serum link Parkinson's disease severity to peripheral inflammation

Yuan Yuan^{1,2†}, Huizhong Li^{1,2†}, Kashyap Sreeram^{1,2†}, Tuyana Malankhanova^{1,2}, Ravindra Boddu^{1,2}, Samuel Strader^{1,2}, Allison Chang^{1,2}, Nicole Bryant^{1,2}, Talene A. Yacoubian³, David G. Standaert⁴, Madalynn Erb⁴, Darren J. Moore⁴, Laurie H. Sanders^{1,5,6}, Michael W. Lutz^{5,6}, Dmitry Velmeshev⁷ and Andrew B. West^{1,2,3,5,7*} 

Abstract

Background LRRK2-targeting therapeutics that inhibit LRRK2 kinase activity have advanced to clinical trials in idiopathic Parkinson's disease (iPD). LRRK2 phosphorylates Rab10 on endolysosomes in phagocytic cells to promote some types of immunological responses. The identification of factors that regulate LRRK2-mediated Rab10 phosphorylation in iPD, and whether phosphorylated-Rab10 levels change in different disease states, or with disease progression, may provide insights into the role of Rab10 phosphorylation in iPD and help guide therapeutic strategies targeting this pathway.

Methods Capitalizing on past work demonstrating LRRK2 and phosphorylated-Rab10 interact on vesicles that can shed into biofluids, we developed and validated a high-throughput single-molecule array assay to measure extracellular pT73-Rab10. Ratios of pT73-Rab10 to total Rab10 measured in biobanked serum samples were compared between informative groups of transgenic mice, rats, and a deeply phenotyped cohort of iPD cases and controls. Multivariable and weighted correlation network analyses were used to identify genetic, transcriptomic, clinical, and demographic variables that predict the extracellular pT73-Rab10 to total Rab10 ratio.

Results pT73-Rab10 is absent in serum from *Lrrk2* knockout mice but elevated by *LRRK2* and *VPS35* mutations, as well as *SNCA* expression. Bone-marrow transplantation experiments in mice show that serum pT73-Rab10 levels derive primarily from circulating immune cells. The extracellular ratio of pT73-Rab10 to total Rab10 is dynamic, increasing with inflammation and rapidly decreasing with LRRK2 kinase inhibition. The ratio of pT73-Rab10 to total Rab10 is elevated in iPD patients with greater motor dysfunction, irrespective of disease duration, age, sex, or the usage of PD-related or anti-inflammatory medications. pT73-Rab10 to total Rab10 ratios are associated with neutrophil degranulation, antigenic responses, and suppressed platelet activation.

[†]Yuan Yuan, Huizhong Li and Kashyap Sreeram contributed equally to this work.

*Correspondence:
Andrew B. West
Andrew.West@Duke.edu

Full list of author information is available at the end of the article



© The Author(s) 2024. **Open Access** This article is licensed under a Creative Commons Attribution 4.0 International License, which permits use, sharing, adaptation, distribution and reproduction in any medium or format, as long as you give appropriate credit to the original author(s) and the source, provide a link to the Creative Commons licence, and indicate if changes were made. The images or other third party material in this article are included in the article's Creative Commons licence, unless indicated otherwise in a credit line to the material. If material is not included in the article's Creative Commons licence and your intended use is not permitted by statutory regulation or exceeds the permitted use, you will need to obtain permission directly from the copyright holder. To view a copy of this licence, visit <http://creativecommons.org/licenses/by/4.0/>. The Creative Commons Public Domain Dedication waiver (<http://creativecommons.org/publicdomain/zero/1.0/>) applies to the data made available in this article, unless otherwise stated in a credit line to the data.

Conclusions The extracellular serum ratio of pT73-Rab10 to total Rab10 is a novel pharmacodynamic biomarker for LRRK2-linked innate immune activation associated with disease severity in iPD. We propose that those iPD patients with higher serum pT73-Rab10 levels may benefit from LRRK2-targeting therapeutics that mitigate associated deleterious immunological responses.

Keywords Inflammation, Single-molecule array assays, Neurodegeneration, Blood-based biomarkers, Transcriptomic analysis

Background

Genetic studies implicate missense mutations and promoter variants in the *leucine-rich repeat kinase 2* (*LRRK2*) gene in Parkinson's disease (PD) risk. Clinical phenotypes associated with *LRRK2* mutations largely overlap with *LRRK2*-negative idiopathic PD (iPD) [1], though carriers of the common G2019S mutation may have a slower motor decline compared to many iPD patients [2]. In genome-wide association studies, the rs76904798 variant in the *LRRK2* promoter increases iPD risk, independent of *LRRK2* missense mutations, while the *LRRK2* N551K/R1398H allele may decrease iPD risk [3, 4]. The role of *LRRK2* in disease progression in iPD is not clear [5]. Biomarkers for *LRRK2* activity, as they may reflect different disease states or change with disease progression, could provide insights into the role of *LRRK2* in disease progression. The *LRRK2* gene (*Lrrk2* in mice and rats) encodes *LRRK2*, a serine/threonine kinase with a tandem Rab-like ROC domain and several known Rab substrates. However, there have been very few studies evaluating *LRRK2*-dependent activity markers in larger cohorts of iPD cases and controls. Since *LRRK2*-targeting drugs have advanced to iPD, a better understanding of which iPD patients to target, and when, may be critical for successful therapeutic development.

LRRK2 phosphorylates several Rab small GTPase substrates that function in the endolysosomal system in different types of cells throughout the body [6]. The *LRRK2* substrate Rab10 is highly expressed in innate immune cells [7]. Activated Rab10 is associated with endolysosomes and has been implicated in endocytosis and vesicle recycling [8, 9]. Both *LRRK2* and Rab10 have been implicated in mycobacteria infection, TLR4 trafficking, and the regulation of ER dynamics and morphology [10, 11]. *LRRK2*-mediated phosphorylation of Rab10 at threonine 73 (i.e., pT73-Rab10) may promote immune signaling pathways, including PI3K-AKT signaling in cell survival and proliferation, by blocking fast-recycling of Rab10-positive vesicles [7]. Of possible relevance to iPD, aggregated α -synuclein may stimulate the production of pT73-Rab10-positive vesicles in microglia, monocytes and macrophages [12]. Though the common pathogenic *LRRK2* mutation G2019S increases autophosphorylated *LRRK2* protein in both mouse models and in vesicle-fractions collected from patient biofluids [13–15], the effects

of G2019S-*LRRK2* on pT73-Rab10 levels have not been clear [16, 17].

Recent reports suggest that *LRRK2* kinase activity in circulating immune cells in the periphery may modify neurodegeneration phenotypes in the brain, though the specific mechanisms underlying these observations, and whether Rab proteins are involved, have not been elucidated [12, 18]. A proportion of *LRRK2* and Rab10 proteins are bound to vesicles including those subject to export into the extracellular space [19, 20]. Our recent results identified higher pT73-Rab10 levels in extracellular vesicle (EV) fractions purified from urine in iPD cases with worse disease phenotypes [21]. However, pT73-Rab10 and total Rab10 proteins were measured in that study by western blots normalized to baseline values, as absolute ratios of pT73-Rab10 to total Rab10 could not be determined using that methodology. Further, past biomarker approaches for *LRRK2* or *LRRK2*-phosphorylated Rab proteins have required large volumes of urine (e.g., >40 mL per subject) or large volumes of freshly-donated blood to isolate and select lysates from certain cell populations or enriched EV fractions. To overcome some of the past challenges associated with high-throughput measures of *LRRK2* activity and Rab phosphorylation in patient samples, here, we develop an ultra-sensitive version of a SiMOA (single-molecule array assay) approach, focusing on the analysis of pT73-Rab10 in serum. With specificity and sensitivity defined in-part through the analysis of serum from well-characterized transgenic mouse and rat strains, our results in both rodents and human samples establish new links between extracellular *LRRK2* levels, pT73-Rab10, and antigenic myeloid cell responses that correlate with worse motor defects in idiopathic PD.

Methods

SiMOA assays

All reagents for the described single-molecule assays used in this study are commercially available. For up-to-date protocols for the measurement of total *LRRK2*, total Rab10, and pT73-Rab10, detailed graphical step-by-step procedures are hosted on Protocols.io and available through the following links:

<https://doi.org/10.17504/protocols.io.dm6gp3188vzp/v1> (total Rab10).

<https://doi.org/10.17504/protocols.io.e6nvwdn69lmk/v1> (pT73-Rab10).
<https://doi.org/10.17504/protocols.io.yxmvm317ol3p/v1> (total LRRK2).

Antibodies used for protein capture include anti-LRRK2 (N241A/34, Antibodies Inc. USA), anti-total Rab10 (clone 605B11, NanoTools, Germany) and anti-pT73-Rab10 (clone MJF-R21, ab231707, Abcam, USA). Detection antibodies include anti-LRRK2 [MJFF2 (c41-2)] (ab172378, Abcam, USA) and anti-Rab10 [MJF-R23] (ab237703, or carrier-free version [recommended] ab238655, Abcam, USA). Antibody stock concentration was determined with a Nanodrop one spectrophotometer (ThermoFisher Scientific, USA). Initial recombinant protein calibrators used in this study that can also be used as protein standards spiked into relevant detection matrices included LRRK2 [G2019S] recombinant human protein (ab177261, Abcam) and recombinant Rab10 (NBP2-23392, Novus Biologicals). All sample incubations, washing, and detection steps are performed on a Quanterix SR-X system and all results analyzed as AEB (average enzymes per bead) values fitted to an optimized non-linear regression curve for each run.

Cell culture and western blots

HEK293T cells grown in DMEM (Gibco, USA) supplemented with 10% fetal bovine serum (Gibco, USA) were transfected with pcDNA3.1-FLAG-LRRK2 and Rab10 plasmids with polyethylenimine hydrochloride (PEI, Polyscience, USA) and lysates harvested ~16-hours later. As indicated, cells were treated with 200 nM MLi2 (Sigma, USA) for 2 h prior to lysis. Cells were lysed in 50mM Tris-HCl pH 8.0 buffer with 150mM NaCl, 1% Triton 100x, and Complete, Protease Inhibitor and PhosSTOP phosphatase inhibitor (Roche, USA). Cell lysates centrifuged at 10 xkg for 10 min at 4 °C, and protein concentration in supernatant determined by BCA assay (Thermo Fisher Scientific, USA).

Mouse bone marrow-derived macrophages (BMDMs) were collected from the femur and tibia from 3- to 5-month-old mice and grown in DMEM (Gibco, USA) supplemented with 10% fetal bovine serum (Gibco, USA) and 100 ng per mL M-CSF (BioLegend, USA). For western blot analysis, cells were lysed directly in 2x Laemmli sample buffer (4% SDS, 20% glycerol, 0.004% bromophenol blue, 0.125 M Tris-HCl-pH6.8, 10% DTT) supplemented with Protease and PhosSTOP inhibitor tablets (Roche, USA).

Samples were electrophoresed on BioRad mini-PROTEAN TGX Stain-Free 4–20%, 15-well gradient gels (BioRad, USA), and transferred to PVDF membranes (Sigma, USA). Phos-tag gels were formulated using the Phos-Tag Common Solution (FUJIFILM Wako, USA) as

recommended by the manufacturer. Separating gels were used with 12% acrylamide and 5 mM Phos-tag reagent along with 1.5 M Tris-HCl, pH=8.8, 10 mM MnCl₂, 10% SDS, 10% ammonium persulfate (APS), and 1% tetramethylethylenediamine (TEMED). Separating gels were cast on BioRad mini-PROTEAN short plates (BioRad, USA). Stacking gels were formulated with 10% acrylamide, 0.5 M Tris-HCl, pH=6.8, 10% SDS, 10% APS, and 1% TEMED. Gels were electrophoresed at constant 100 V for approximately 2 h, soaked in a running buffer supplemented with 1 mM EDTA, and then transferred to PVDF. Primary antibodies utilized include pT73-Rab10 (ab231707, abcam), total-Rab10 (ab237703, Abcam, USA), and total-LRRK2 (N241 75–253, nanoTools GmbH & Co., Germany).

Procedures in rodents

Animal protocols were approved by local Animal Care and Use Committees accredited by the AAALAC. Tg-WT-*Lrrk2* (JAX stock #012466), Tg-G2019S BAC-*Lrrk2* (JAX stock #012467), *Lrrk2*^{R1441C/R1441C} (JAX stock #009346), *VPS35*^{WT/WT}, *VPS35*^{WT/D620N} and *VPS35*^{D620N/D620N} (JAX stock #023409), *Lrrk2*^{-/-} knock-out (JAX stock #016121), C57BL/6J (JAX stock #000664), BL/6-CD45.1 (JAX stock#002014), *Sncα*^{-/-} (JAX stock #016123) and PAC-SNCA/*Sncα*^{-/-} (JAX stock #010710) strains were obtained from Jackson Laboratories. CD1 (CR #022CD1) mice and outbred Long Evans *Lrrk2*^{+/+} rats were obtained from Charles River Laboratories. *Lrrk2* knock-out Long-Evans rats were obtained from Envigo. Venous serum was collected in mice via facial vein draws, and in rats via lateral saphenous vein draws, each into microtainer serum collection tubes (Becton Dickinson, USA). 30 min post-collection, tubes were centrifuged at 8 xkg for 5 min at RT and serum supernatants aliquoted and stored at -80 °C. Serum samples with less than 40 μL available, or showing evidence of extensive hemolysis of more than 100 mg per dL hemoglobin, as estimated by standard scales, were excluded from further analysis.

The small molecule LRRK2 kinase inhibitor PFE-360 (PF-06685360, Pharmaron, USA) was administered to rodents in a suspension solution consisting of deionized water and 0.5% (w/v) methylcellulose (Sigma, USA). Drug solutions were made the day before administration with 4 °C incubation overnight with stir-bar mixing. Formulations were administered with 18-gauge curved 2.4 mm ball point stainless feeding needles (KVP International, USA). Rodents were dosed at 10 mg per kg. The drug suspension was prepared at 1 mg per mL for mice and 5 mg per mL for rats.

For whole body irradiation, mice were exposed to 11 grays (split into two equal doses separated by 3 h) using a Xstrahl CIX3 Xray irradiator and maintained on

acidified-antibiotic water consisting of NaOCl, HCl, and neomycin sulfate for 6 days. For bone marrow transplantation, donor mouse cells were isolated from femur and tibia washes with a 26 gauge needle and RPMI1640 media (Gibco, USA) and filtered through a 70 μm cell strainer as described [22]. After centrifugation at 300 $\times g$ for 10 min at 4 $^{\circ}\text{C}$, cell pellets were treated with ammonium-chloride-potassium (ACK) lysis buffer (Gibco, USA). Pelleted cells were then resuspended into fresh RPMI1640 media and immediately transplanted (tail vein injection) with $3\text{--}5 \times 10^6$ bone marrow mononuclear cells after the second dose of radiation in the host mice. Transplanted mice were maintained on the acidified-antibiotic water for 4 weeks.

Flow cytometry analysis of mouse blood was accomplished with freshly collected blood (via facial vein puncture) with RBC lysis for 10 min at RT in ACK solution, and centrifugation at 300 $\times g$ for 10 min at 4 $^{\circ}\text{C}$ as described [23, 24]. Leukocyte pellets were washed and suspended in buffer (PBS, 0.5% bovine serum albumin, and 0.01% sodium azide), blocked with Fc γ receptor antibody (clone 2.4G2, eBioscience, USA), and cells stained with brilliant violet-CD45 (clone 30-F11, Biolegend, USA); allophycocyanin-conjugated-CD45.1 (clone A20, eBioscience, USA); fluorescein isothiocyanate-conjugated-CD45.2 (clone 104, eBioscience, USA); allophycocyanin-conjugated Ly6G (Gr-1, clone 1A8, eBioscience, USA); eFlour 450-conjugated Ly6C (clone HK1.4, eBioscience, USA) and fluorescein isothiocyanate-conjugated CD4 (clone GK1.5, eBioscience, USA). 7-aminoactinomycin D (00-6993-50, Invitrogen, USA) was used for live-dead staining and analyzed on an Attune NxT acoustic focusing instrument (ThermoFisher Scientific, USA) and FlowJo 10.8.1 software (Becton Dickinson, USA).

For polymicrobial sepsis induction, 200 μL of a rapidly thawed cecal slurry preparation was injected intraperitoneal in mice, with serum collections 8 and 72 h (as indicated) post injection. For the cecal slurry preparation, cecal contents were harvested and pooled from 25 male CD1 mice and mixed at a ratio of 0.5 mL of water to 100 mg of cecal contents, sequentially filtered through a 860 μm , 190 μm and 70 μm mesh (Fisher Scientific, USA), and then added to an equal volume of 30% glycerol in PBS as described [25]. Samples were submitted to the University of North Carolina Microbiome Core Facility (supported in part by NIH grant P30 DK34987) for 16S rRNA amplicon sequencing. To determine colony formation unit (CFU) per mL, slurries were plated onto brain-heart-infusion broth agar plates (1.5% agar) and incubated for 24 h at 37 $^{\circ}\text{C}$ in ambient air.

Human subjects, clinical, and demographic data

This study was approved by local Institutional Review Boards and all participants signed informed consents.

All coded serum samples were processed by investigators blinded to sample identity, and final curated datasets were achieved before associating clinical and demographic characteristics were assigned to biomarker values. Serum was obtained from participants (Table 1) all enrolled at a single site at the University of Alabama at Birmingham (UAB) Movement Disorder Clinic, part of the Parkinson's Disease Biomarker Program (<http://pdbp.ninds.nih.gov>). Participants were selected based on frequency matching of age and gender between cases and controls, with inclusion for cases based on United Kingdom Parkinson's Disease Society Brain Bank Criteria. Inclusion criteria for healthy controls were aged 35 to 85 years, lack of PD in first-degree blood relatives, and a lack of positive responses on more than 3 items in the PD Screening Questionnaire [26]. Exclusion criteria for all subjects included atypical features indicative of progressive supranuclear palsy, multiple system atrophy, corticobasal degeneration, cerebellar signs, supranuclear gaze palsy, apraxia, disabling autonomic failure, neuroleptic treatment at time of onset of parkinsonism, active treatment with a neuroleptic at time of study entry, history of repeated strokes with stepwise progression of parkinsonism, history of repeated head injury, history of definite encephalitis, dementia, known severe anemia, or kidney disease as determined by measurement of serum creatinine and/or medical records, infections, or any serious comorbidity that would interfere with participation in the study. Demographics, PD characteristics, medications, medical history, and family history of PD were collected. Levodopa equivalent daily dose was calculated as described [26]. Serum samples were collected according to BioSpecimen Exchange for Neurology Disorders (BioSEND) protocol. Venous blood was collected in red-capped BD Vacutainer serum tubes that were incubated at RT for 30 min, and then centrifuged for 15 min at 1500 $\times g$ at 4 $^{\circ}\text{C}$. Serum samples demonstrating more than 100 mg per dL hemoglobin estimated by visual inspection against colorimetric scales were excluded from analysis. Resultant supernatants were aliquoted and stored at -80 $^{\circ}\text{C}$ until further use. Venous blood was next collected into PAXgene blood RNA tubes (IVD, Qiagen, USA) following manufacturer's recommended protocol. Samples and all clinical data including the MDS-UPDRS were collected between 08:00 and 12:00 in the day with PD patients taking their usual medications. All clinical and demographic data collected from these participants has been deposited into the Data Management Resource managed and available from the National Institutes of Health (DMR, <https://pdbp.ninds.nih.gov/portal>).

Serum processing and proteomic analysis

Some serum samples were processed using Exo-Spin serum mini column exosome purification kits (Cell

Table 1 Demographics, clinical information, and biomarker data in subjects recruited into the Parkinson's disease biomarker program (PDBP)

Cohort feature	Male (N=276)			Female (N=246)		
	PD (N=187)	HC (N=89)	p*	PD (N=90)	HC (N=156)	p*
Disease duration, Mean years (SD)	8.1 (5.9)	0	<0.0001	6.5 (4.5)	0	<0.0001
Age, Mean years (SD)	64.0 (9.6)	61.0 (13.2)	0.259	63.9 (8.8)	59.6 (9.9)	0.001
MDS-UPDRS I, Mean (SD)	10.8 (5.9)	5.1 (4.5)	<0.0001	11.8 (6.1)	5.4 (4.0)	<0.0001
MDS-UPDRS II, Mean (SD)	14.6 (8.1)	1.3 (2.6)	<0.0001	12.8 (8.3)	0.9 (2.1)	<0.0001
MDS-UPDRS III, Mean (SD)	29.1 (13.4)	0.3 (1.0)	<0.0001	24.5 (11.1)	0.2 (0.7)	<0.0001
MDS-UPDRS IV, Mean (SD)	1.8 (3.2)	0	<0.0001	1.9 (2.9)	0	<0.0001
MDS-UPDRS Total, Mean (SD)	56.4 (24.2)	6.9 (6.8)	<0.0001	50.9 (21.1)	6.4 (5.7)	<0.0001
MoCA, Mean (SD)	24.0 (3.5)	25.5 (3.0)	0.001	25.1 (3.0)	27.1 (1.9)	<0.0001
UPSIT, Mean (SD)	18.3 (7.3)	30.9 (6.0)	<0.0001	20.4 (8.1)	34.3 (4.1)	<0.0001
Epworth Sleep Scale, Mean (SD)	9.9 (4.7)	6.6 (3.6)	<0.0001	9.1 (5.2)	5.2 (3.2)	<0.0001
NSAID use, N (%)	84 (45)	28 (31)	0.036	36 (40)	46 (29)	0.095
Statin use, N (%)	60 (32)	31 (35)	0.682	25 (28)	40 (26)	0.765
LEDD, Mean (SD)	561 (500)	0	<0.0001	513 (757)	0	<0.0001
Family history of PD, N (%)	49 (26)	7 (8)	0.0003	27 (30)	9 (6)	<0.0001
Serum biomarkers and characteristics						
Sample days-in-freezer, Mean (SD)	2214 (364)	2240 (338)	0.671	2296 (335)	2184 (344)	0.007
Total LRRK2, ng/mL, Median (IQR)	0.77 (2.04)	0.50 (1.40)	0.034	0.49 (2.43)	0.50 (1.16)	0.318
Mean	12.05	4.36		3.24	3.07	
95%CI [LL, UL]	[-1.93, 26.02]	[2.08, 6.65]		[1.87, 4.63]	[1.33, 4.81]	
pT73-Rab10, ng/mL, Median (IQR)	1.09 (8.81)	0.68 (5.77)	0.252	1.19 (9.45)	0.28 (2.36)	0.073
Mean	17.36	11.83		8.69	5.70	
95%CI [LL, UL]	[7.00, 27.72]	[5.59, 18.07]		[5.03, 12.35]	[3.49, 7.91]	
Rab10, ng/mL, Median (IQR)	7.69 (40.67)	8.01 (25.46)	0.491	10.51 (47.12)	5.68 (12.65)	0.012
Mean	115.45	66.22		68.24	45.77	
95%CI [LL, UL]	[60.99, 169.90]	[29.69, 102.75]		[38.00, 98.48]	[23.31, 68.23]	
pT73-Rab/Rab10, %, Median (IQR)	10.1 (23.8)	8.8 (20.57)	0.260	7.2 (17.8)	6.2 (14.2)	0.452
Mean	17.6	15.2		14.2	12.6	
95%CI [LL, UL]	[14.5, 20.7]	[10.8, 19.6]		[10.3, 18.2]	[9.6, 15.6]	

MDS-UPDRS, Movement Disorders Society-Unified Parkinson's Disease Rating Scale, part I-IV; MoCA, The Montreal Cognitive Assessment; UPSIT, University of Pennsylvania Smell Identification Test; LEDD, L-dopa Equivalent Daily Dosage; SD, standard deviation; IQR, interquartile range; CI, confidence interval; LL, lower limit of confidence interval; UL, upper limit of confidence interval

*p values are from 2-tailed t-tests for all continuous cohort variables and Fisher's exact test for cohort categorical variables. P values from serum biomarkers (non-transformed) are from Mann-Whitney tests

Guidance Systems LLC, USA), where 100 μ l of serum samples were centrifuged at 300 \times g for 10 min at 4 $^{\circ}$ C to remove any large debris and then at 16 \times g for 30 min, and supernatant was transferred to the PBS-equilibrated columns. The first flow-through was discarded, and another 180 μ L of PBS was added to the top of the column, centrifuged at low speed 20 \times g for 1 min, fraction 1 collected, and this procedure was repeated two more times. 100 μ g of protein (BCA analysis) was processed and evaluated on a Thermo Orbitrap Fusion Lumos mass spectrometer coupled with ultra-performance liquid chromatography (Thermo Fisher, USA). Tandem mass spectra were extracted and all samples were analyzed using Sequest set to search MasterMix_011320.fasta; SP_Hsapiens_082922.fasta. Scaffold (version Scaffold_5.2.2, Proteome Software Inc., USA) was used to validate MS/MS based peptide and protein identifications, where peptide identifications were accepted if they

could be established at greater than 92.0% probability to achieve an FDR less than 1.0% by the Percolator posterior error probability calculation [27]. Protein identifications were accepted if they could be established at greater than 99.0% probability to achieve an FDR less than 1.0% and contained at least 2 identified peptides. Protein probabilities were assigned by the Protein Prophet algorithm [28].

Whole blood transcriptomics and weighted gene network correlation analysis

RNA-Seq was performed through the Accelerating Medicines Partnership-Parkinson's Disease (AMP-PD) pipeline. RNA samples were rRNA and globin depleted via the Globin-Zero Gold kit (Illumina, USA) and first-strand synthesis and second strand synthesis were performed using the Ultra II First Strand Module and Ultra II Directional Second Strand Module (New England Biolabs, USA). Following second strand synthesis, the

double-stranded cDNA was converted to a sequencing library by standard, ligation-based library preparation (see <https://amp-pd.org/transcriptomics-data>). Following ligation to standard paired-end adaptors (Illumina, USA), each library was amplified for 12 cycles using Kapa HiFi polymerase (Roche, USA), with forward and reverse primers including a 8 nucleotide unique index sequence. Insert sizes were evaluated via Caliper GX (Perkin-Elmer, USA) and libraries quantitated with Kapa SYBR FAST Universal kit (Roche, USA). Sequencing was performed on the Illumina NovaSeq 6000 platform to generate 100 M paired reads per sample at 150 nucleotide read lengths. Samples were demultiplexed based on the unique i5 and i7 indices to individual sample FASTQ files. Only participants with full featureCounts were included here which was $n=522$. The featureCounts matrix was filtered to include all genes with non-zero transcript counts in greater than 25% of samples ($n=36,168$). A variance stabilizing transformation (VST) was applied using the DESeq2 V1.40.2 package [29]. DESeq2 was also utilized for differential analysis of count data in PD versus control subjects to identify differentially expressed genes (DEGs), where Benjamini-Hochberg corrected p values of <0.05 are considered significant.

The “WGCNA” R package was utilized to construct networks of coexpressed genes, where each node corresponds to a gene expression profile, and edges are determined by pairwise correlations between gene expression profiles across samples. A co-expression similarity matrix was constructed by calculating correlations among significant genes, which was converted to the adjacency matrix using a thresholding procedure. The optimal power coefficient β was identified by the R function `pickSoftThreshold`. A topological overlap matrix (TOM) was generated by the adjacency matrix, representing the strength of gene-gene interactions. Alongside hierarchical gene clustering trees, the TOM identifies large modules connected to different colors. Module eigengenes (i.e. a weight average expression profile) were determined from the first principal component of each module, and significant modules were selected from module-trait relationships between eigengenes and pT73-Rab10 to total Rab10 ratios (adjusted $p < 0.05$ considered significant). This analysis was repeated for LRRK2 serum levels and MDS-UPDRS III scores. Predicted protein-protein interaction networks in the modules were generated with StringDB (<http://string-db.org>). K-means clustering ($n=10$ clusters) was performed and clusters with the highest average local clustering coefficient were visualized. Reactome pathway ontological terms for the top cluster were also generated using StringDB.

Statistical analysis software

GraphPad Prism 10, JMP Pro 16, and R-4.3.1 were utilized for all statistical tests. Types of statistical analyses used are indicated in Figure legends in addition to the numbers and types of independent observations that compose each experiment. All raw data associated with the figures are available online as Supplemental Material 1.

Results

Development of sensitive and specific scalable assays for the measurements of the ratio of pT73-Rab10 to total Rab10 and LRRK2 in serum

Recent single molecule array (SiMOA) assays have been developed that successfully measure, to femtomolar levels, pathology biomarkers in neurodegenerative diseases from low volumes of biobanked serum or plasma [30]. Scalable assays for the measurement of the ratio of pT73-Rab10 to total Rab10 in biobanked biofluids have not previously been described. To fill this gap, we first screened efficiencies of different monoclonal antibody pairs for the detection of recombinant LRRK2 and Rab10 proteins in the SiMOA format. We, and others, have previously defined specificity of these antibodies in western blot formats using lysates from knockout or knockdown of LRRK2 and/or Rab proteins [7, 31]. With the selected antibody pairs indicated in Fig. 1A, B, alignments of the antibody-recognized epitopes onto AlphaFold structures showed solvent-oriented positioning with sufficient space between epitopes to allow simultaneous binding. Using recombinant full-length proteins for Rab10 and LRRK2 (Fig. 1C), standard curves were developed in custom-formulated sample buffers (e.g., “sample diluent buffer”). As both LRRK2 and pT73-Rab10 interact at the membrane in complex, and these proteins may be associated inside of extracellular vesicles, sample buffers were supplemented with denaturants (i.e., sodium deoxycholate) and reducing agents (i.e., dithiothreitol) not typically included in single-molecule assays. These additives might help dissociate membranes and complexes while still allowing antibody binding to the desired epitopes. In the denaturing sample diluent buffer matrix, we could achieve sensitivity for the detection of recombinant Rab10 and LRRK2 proteins that reached low picogram per milliliter (Fig. 1D, E).

As recombinant proteins may not mimic realistic matrix conditions (e.g., cell lysates, or viscous serum samples), LRRK2-transfected cell lines were processed and analyzed to determine the performance of the assay in the complexity of total protein lysates. First, a phos-tag approach was used to resolve the proportion of Rab10 phosphorylated according to western blot analysis of HEK-293T cells transfected with both FLAG-R1441G-LRRK2 with human FLAG-Rab10. Similar to proportions

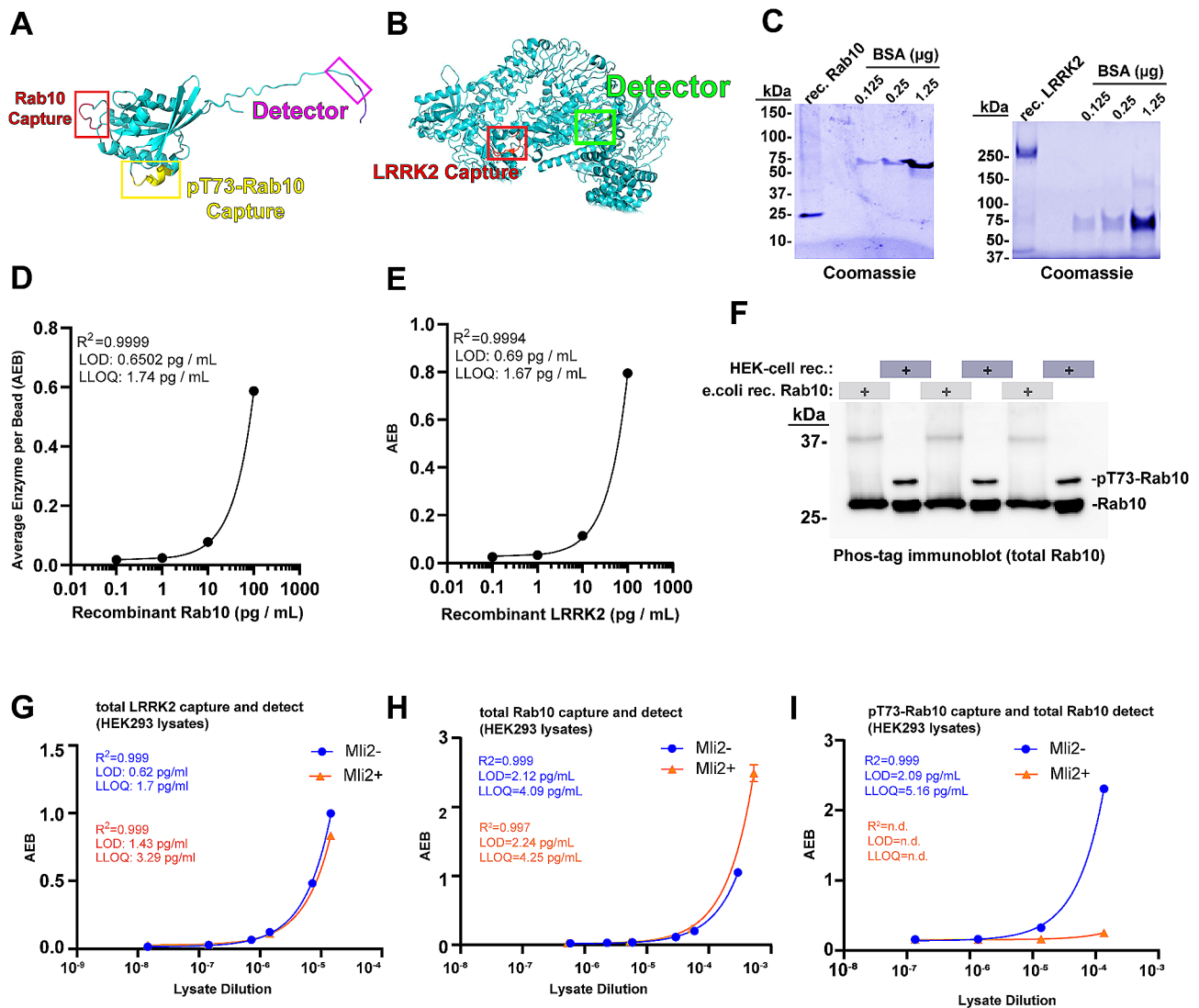


Fig. 1 Development of sensitive single-molecule array assays and standards for fluid measures of total LRRK2, total Rab10, and pT73-Rab10. **(A)** AlphaFold structure of Rab10 and **(B)** LRRK2. Specific epitopes selected for the quantification of total LRRK2, total Rab10, and pT73-Rab10. The assay for Rab10 and pT73-Rab10 share the same detector antibody on the C-terminus but differ in capture antibody epitopes. **(C)** Representative SDS-PAGE gels with Coomassie stain (blue) for the quantification of recombinant His-Rab10 (derived from *E. coli* cells) and FLAG-G2019S-LRRK2 (derived from HEK-293T cells). Recombinant bovine-serum albumin standards are shown. **(D)** Representative regression curves for the measurement of recombinant Rab10 and **(E)** recombinant LRRK2 in the assay buffer. Goodness-of-fit (r -squared), limit-of-detection (LOD), and lower-limit of quantification (LLOQ) are indicated and calculated from duplicate and triplicate values for each assay point. **(F)** Representative phos-tag immunoblot analysis showing the proportion of Rab10 protein phosphorylated in protein lysates. HEK-293T lysates were generated through transient transfection of plasmids expressing FLAG-R1441G-LRRK2 with human FLAG-Rab10. The ratio of pT73-Rab10 to total Rab is calculated from three independent preparations as $15.2\% \pm 0.9\%$ SEM. Protein preparations analyzed by phos-tag analysis are utilized as standards for single-molecule arrays (SiMOA). **(G)** Representative regression curves for the analysis of LRRK2, **(H)** Rab10, and **(I)** pT73-Rab10, as measured in diluted (sample buffer) HEK-293T protein lysates. Prior to lysis, cells were treated with Mli2 (200 nM, 30 min, red dots and lines) or vehicle (blue dots and lines). Assay quality parameters (orange font) are indicated based on triplicate values. Error bars for experimental replicates are typically less than 5% and too short to be visualized graphically in most of the plots

measured in previous reports [17, 32], $15.2 \pm 0.9\%$ of total Rab10 was found phosphorylated in the lysates (Fig. 1F). The SiMOA assays reported the concentration of LRRK2 protein and total Rab10 protein at $14.48 \pm 0.67 \mu$ g per mL for LRRK2 and $5.88 \pm 1.52 \mu$ g per mL (SEM) for total Rab10 in the lysates (Fig. 1G, H). Based on the measured proportion of pT73-Rab10 relative to

non-phospho-Rab10 protein, the concentration of pT73-Rab10 in the lysate standard measured $0.89 \pm 0.23 \mu$ g per mL. Lower limits of detection and quantification in the lysates were slightly worse than those calculated for recombinant proteins (Fig. 1G-I). The analysis of pT73-Rab10 levels in HEK293T cells treated with the LRRK2 kinase inhibitor Mli2 prior to lysis shows that

the pT73-Rab10 assay does not significantly cross react with non-phosphorylated Rab10 protein, even with high Rab10 levels in the lysates (Fig. 11).

To determine whether these assays are viable in serum, known picogram quantities of recombinant LRRK2 and Rab10 were spiked into human serum samples and analyzed for recovered protein (after background subtraction). Both LRRK2 and Rab10 were recovered to ~75% in serum, consistent with good assay performance (Supplemental Fig. S1A, B). A spike-in experiment using serum procured from *Lrrk2* knockout (*Lrrk2*^{-/-}) mice showed similar recovery of detection (Supplemental Fig. S1C). Higher signal (average enzyme per bead, or AEB) in the human serum samples that lacked any added recombinant proteins suggested the presence of endogenous LRRK2 and Rab10 proteins in serum.

To establish specificity of the assay signals in serum, LRRK2, Rab10 and pT73-Rab10 proteins were measured from low-volume single facial vein draws (~40–60 μ L) from a cohort of wild-type C57BL6/J mice, *Lrrk2*^{-/-} mice, or *Lrrk2*^{R1441C/R1441C} knockin mice (Fig. 2A). Serum LRRK2 protein levels could not be determined in the *Lrrk2*^{-/-} mice due to levels below limits of detection (Fig. 2A), but were detectable in the other strains, suggesting good specificity for the LRRK2 assay. Serum Rab10 levels were similar between strains (Fig. 2B), demonstrating LRRK2 does not significantly regulate extracellular concentrations of total Rab10 levels in serum. pT73-Rab10 levels in *Lrrk2*^{-/-} mice could not be determined, whereas the mean of the ratio of pT73-Rab10 to total Rab10 was low ($0.79\% \pm 0.08\%$) in non-transgenic C57BL6/J mice. Notably, three of nineteen wild-type C57BL6/J mice had ratios of pT73-Rab10 to total Rab10 that were below the measured assay lower-limits of quantification (Fig. 2C). However, the ratio of pT73-Rab10 to total Rab10 was measurable in all *Lrrk2*^{R1441C/R1441C} knockin mouse serum samples, and, on average, was approximately twice that of wild-type C57BL6/J mice (Fig. 2C). These results suggest that wild-type mice have a very low basal state of phosphorylated Rab10 in serum, sometimes undetectable, where less than 1% of total Rab10 protein presents in the phosphorylated state. Measured ratios in both the C57BL6/J and *Lrrk2*^{R1441C/R1441C} mice were variable but appeared to be normally distributed (Fig. 2C).

The effects of the pathogenic G2019S-LRRK2 mutation on pT73-Rab10 levels has been controversial, with some studies showing G2019S-LRRK2 does not increase phosphorylated Rab10 levels over WT-LRRK2 [16, 17, 21]. Our previous work measuring LRRK2 and pT73-Rab10 proteins using western blots demonstrated that peripheral macrophages isolated from transgenic mouse-BAC Tg-WT-*Lrrk2* and Tg-G2019S-BAC *Lrrk2* mice have similar levels of total LRRK2 protein compared to peripheral

macrophages isolated from human blood, with non-transgenic mice and *Lrrk2* knockin mice showing much lower levels of LRRK2 protein, irrespective of interferon-stimulation of *LRRK2/Lrrk2* expression [12]. Analysis of serum from Tg-G2019S-BAC *Lrrk2* mice show, on average, increased extracellular LRRK2 protein compared to Tg-WT-BAC *Lrrk2* mice (Fig. 2D), but similar levels of total Rab10 (Fig. 2E). Serum from Tg-G2019S-BAC *Lrrk2* mice shows much higher ratios of pT73-Rab10 to total Rab compared to wild-type or *Lrrk2* knockin mice, averaging $15.1 \pm 1.4\%$ of total Rab10 phosphorylated (Fig. 2F). In comparison to Tg-G2019S-BAC *Lrrk2* serum, Tg-WT-BAC *Lrrk2* serum shows about half the amount of phosphorylated Rab10 on average ($7.7 \pm 1.2\%$). These results show extracellular pT73-Rab10 is sensitive to LRRK2 expression and the G2019S-LRRK2 mutation.

To further explore the effects of different pathogenic *LRRK2* mutations on the ratio of pT73-Rab10 to total Rab10, HEK-293T cells were transfected with FLAG-WT-LRRK2, R144G, Y1699C, and G2019S-LRRK2, and verified for pT73-Rab10 levels with traditional western blot analysis (Fig. 2G, H). The activating effects of G2019S-LRRK2 on autophosphorylated pS1292-LRRK2 were confirmed by western blot. The SiMOA assay measured $23.9 \pm 2.6\%$ and $17.9 \pm 1.8\%$ phosphorylated Rab10 for R1441G and Y1699C-LRRK2, respectively, in comparison to $7.1 \pm 0.9\%$ for WT-LRRK2 (Fig. 2I). However, G2019S-LRRK2 expression in cell lysates did not increase pT73-Rab10 to total Rab10 ratios over those measured with WT-LRRK2 expression.

The extracellular ratio of pT73-Rab10 to total Rab10 primarily derives from bone-marrow immune cells and increases with inflammation

According to recent transcriptomic studies, the highest *LRRK2* mRNA levels in cells and tissues across the body may reside in myeloid cell populations, particularly neutrophils, monocytes and macrophages, and microglia [12, 33, 34]. Circulating myeloid cells can be efficiently ablated with a single whole-body irradiation procedure (Fig. 3A). In CD-1 outbred mice, six days after irradiation, there were few leukocytes left in blood. In these irradiated mice, LRRK2 protein in serum drops to near undetectable levels (Fig. 3B), and both total Rab10 as well as the ratio of pT73-Rab10 to total Rab10 drops considerably compared to baseline (Fig. 3C, D). Transplantation of bone-marrow cells back to the irradiated mice re-establishes leukocyte population counts in the blood (Fig. 3E). In the transplanted mice, normal serum levels of LRRK2 and the ratio of pT73-Rab10 to total Rab10 were measured (Fig. 3F-H). These results suggest that the ratio of pT73-Rab10 to total Rab10 in serum primarily originates from bone-marrow derived cells.

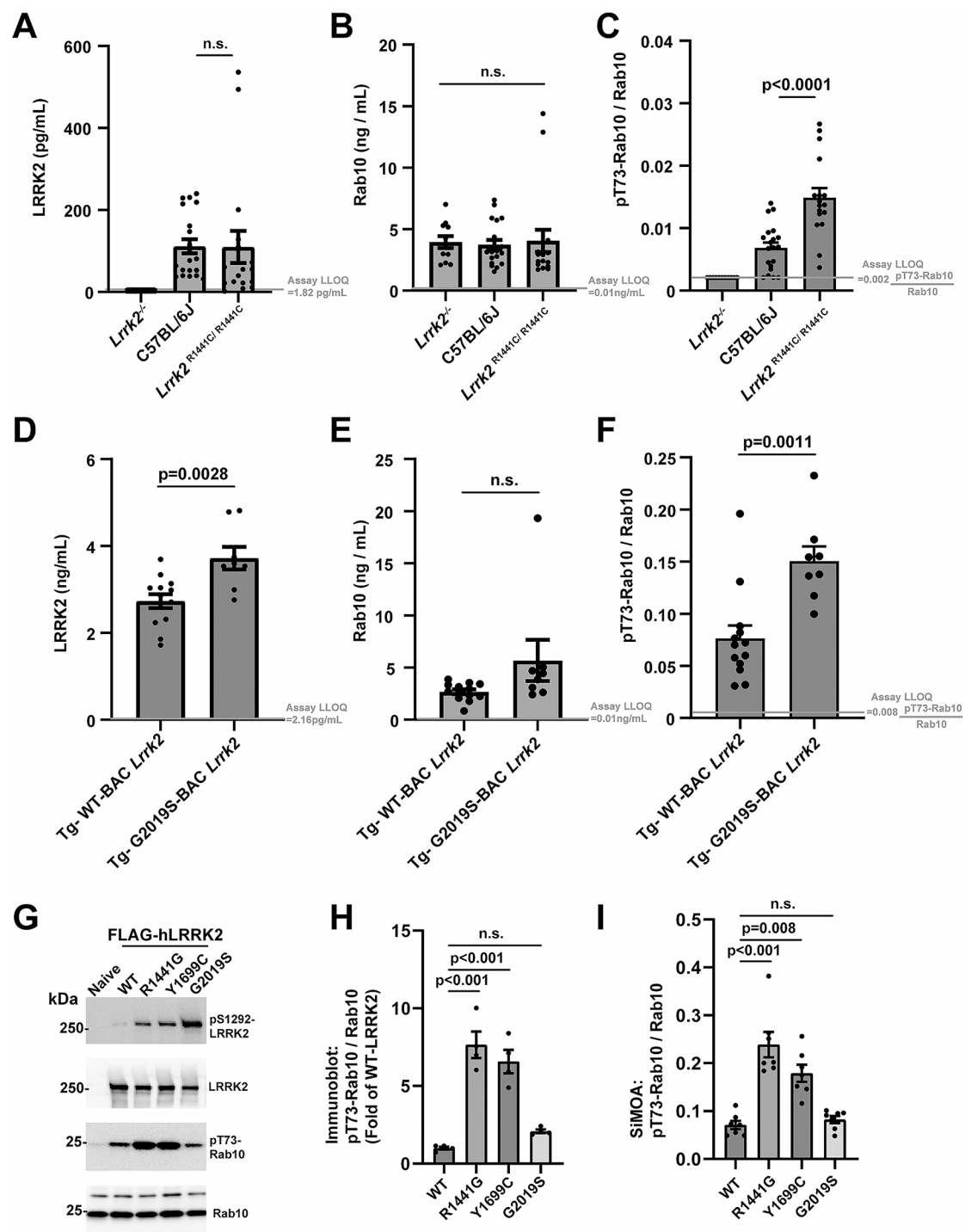


Fig. 2 *LRRK2* mutations increase the extracellular ratio of pT73-Rab10 to total Rab10 as measured with single-molecule array assays (SiMOA) in serum. **(A)** Levels of total LRRK2, **(B)** total Rab10 and **(C)** the ratio of pT73-Rab10 to total Rab10 as measured by SiMOA in venous mouse serum from *Lrrk2*^{-/-} (8 males and 3 females), non-transgenic C57BL/6J (12 males and 8 females), and knockin *Lrrk2*^{R1441G/R1441G} mice (9 males and 8 females). **(D-F)** A cohort of transgenic Tg-WT-BAC *Lrrk2* (4 males and 9 females) and Tg-G2019S-BAC *Lrrk2* mice (5 males and 3 females) were also analyzed for these markers. In these strains, no differences were noted between males and females. Ages in both cohorts of the mice ranged from 3–6 months. **(G)** Representative immunoblots of lysates from HEK-293T cells transfected with FLAG-LRRK2 plasmids 24-hours before harvesting lysates. **(H)** Quantification of endogenous pT73-Rab10 to total Rab10 ratio. **(I)** SiMOA assay analysis of the lysates for the ratio of pT73-Rab10 to total Rab10. Dots show mean values calculated from independent experiments. Columns show group means, error bars show SEM, and p values are determined with two-tailed t-tests, or from one-way ANOVA followed by Tukey's post-hoc test in the graphs with more than two groups

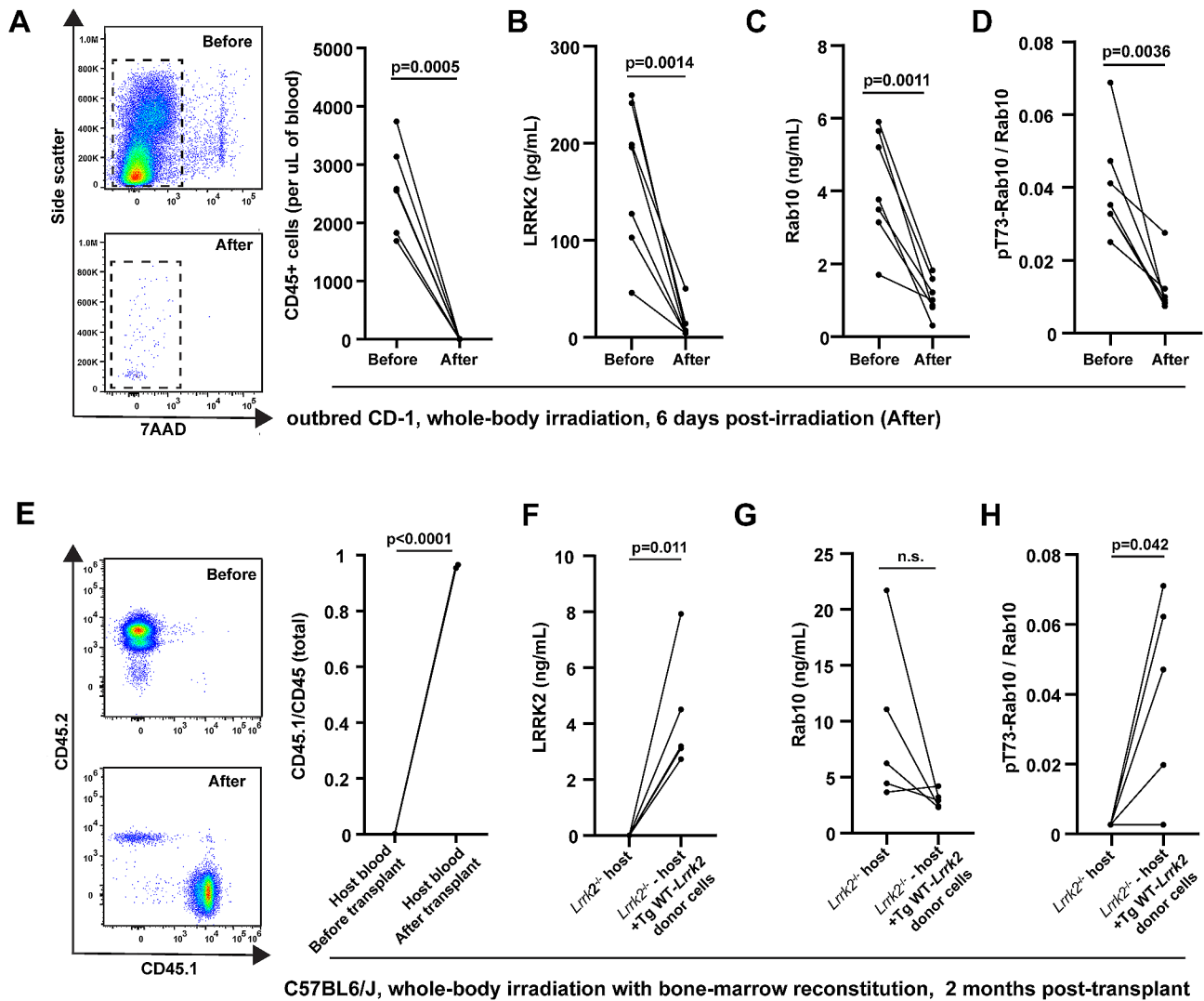


Fig. 3 Serum LRRK2 and pT73-Rab10 proteins originate primarily from bone marrow immune cells. **(A)** Representative cytographs and column graphs showing the analysis of live (7AAD- 7-Aminoactinomycin D negative) leukocytes in blood from outbred male CD-1 mice before and six-days after 11 grays of radiation. **(B)** SiMOA analysis of serum from these mice for **(B)** total LRRK2, **(C)** total Rab10 and **(D)** the ratio of pT73-Rab10 to total Rab10. **(E)** Cytographs show the analysis of host CD45.2 and donor CD45.1 mice before and after radiation, and the column graph shows the mean of the ratio of CD45.1 cells to total CD45 cells ($n=3$ male mice). Bone marrow transplantation of donor Tg-WT-*Lrrk2* cells into host *Lrrk2*^{-/-} mice restores levels of **(F)** total LRRK2, **(G)** total Rab10 and **(H)** the ratio of pT73-Rab10 to total Rab10. Each dot shows mean values from the analysis of a single animal (all ~ 2 months of age), and p values are calculated from paired (before and after) sample t-tests

Our and other previous work suggests *LRRK2* expression may increase in myeloid cells after exposures to lipopolysaccharide or interferon-induction as part of a pro-inflammatory response [35, 36]. The role of phosphorylated Rabs such as pT73-Rab10 in these responses is not yet clear, though our recent studies in macrophages implicate pT73-Rab10 in blocking signaling endosomes from turnover in canonical AKT pathways [7]. To test whether acute and systemic inflammation in mice might affect extracellular pT73-Rab10 to total Rab10 ratios, we introduced a polymicrobial sepsis challenge to outbred CD-1 mice that caused large increases in serum concentrations of IFN γ and TNF (Fig. 4A-C). Surprisingly,

72-hours post sepsis, serum LRRK2 levels only modestly increase in female mice, and not at all in male mice (Fig. 4D). As IFN γ is thought to be a principal driver of LRRK2 expression in myeloid cells [37], higher IFN γ levels that develop in female mice may explain higher extracellular LRRK2 levels, though larger group sizes may be needed for definitive correlations due to the variable responses to sepsis in these outbred mice. Further, septic shock drops the levels of total Rab10 in serum (Fig. 4E). However, the measured ratio of pT73-Rab10 to total Rab10 increases in both male and female mice (Fig. 4F). These results show that the ratio of pT73-Rab10 to total Rab10 in serum increases with sepsis, albeit with

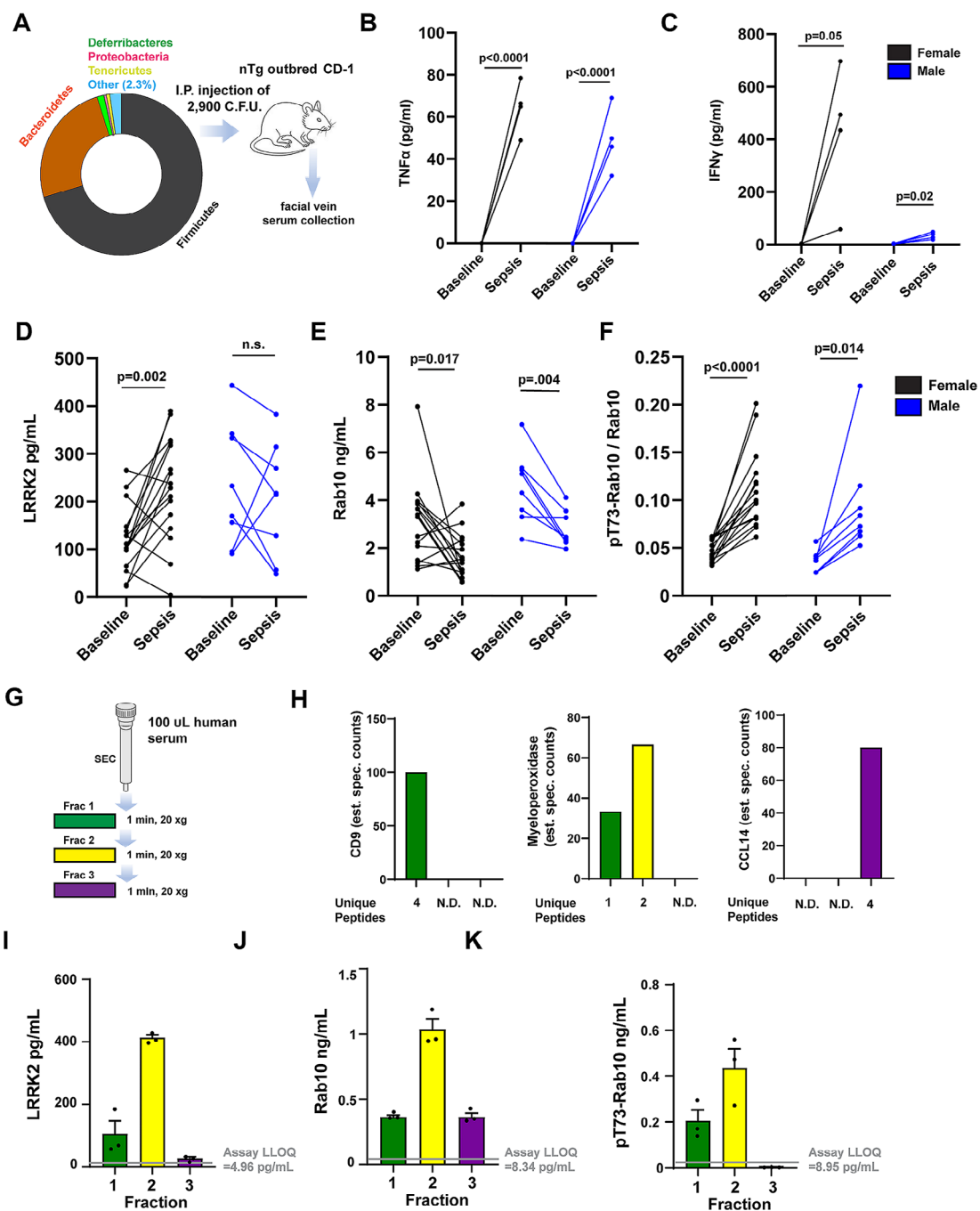


Fig. 4 Sepsis increases the extracellular ratio of pT73-Rab10 to total Rab10 in serum that primarily localizes to exosome-enriched serum fractions. **(A)** Microbe profile of cecal slurry generated from healthy CD-1 outbred male mice. Percentages of phylum-level taxonomy, identified by 16S rRNA amplicon sequencing, are depicted with the “Other” category including *Actinobacteria*, *Cyanobacteria*, and *Verrococcinobacteria*. Slurries were injected intraperitoneally into a cohort of outbred male ($n = 8$) and female ($n = 16$) CD-1 mice, with serum procured from facial vein draws. At the 8 hr time point after injection, 4 female and 4 male mice were selected at random to measure serum **(B)** interferon- γ (IFN γ) and **(C)** TNF with ELISA analysis. **(D)** Before and after graphs show changes in serum LRRK2 levels, **(E)** total Rab10 and **(F)** the ratio of pT73-Rab10 to total Rab10 72 hrs post-injection. P values shown are from paired samples (before and after) t-tests. **(G)** Procedure for “Exo-Spin Serum mini columns” size-exclusion fractionation of 100 microliters of human serum spread into fractions 1–3. **(H)** Proteomic analysis of eluted fractions via mass spectrometry assessments of the relative abundance of unique peptides associated with characteristic serum exosome proteins CD9 (plasma-membrane protein enriched in exosomes and extracellular vesicles), myeloperoxidase (a soluble myeloid-cell produced enzyme enriched in exosomes and extracellular vesicles), and a small soluble cytokine HCC-1 (CCL14). **(I)** Column graphs show levels of LRRK2, **(J)** Rab10, **(K)** and pT73-Rab10 as measured in three different human biobanked serum samples (one male and one female with PD, and one healthy control). Green bars are measured from fraction one, yellow bars are fraction two, and purple are fraction three. Columns show group mean and error bars show SEM

large variability between animals. One each of the wild-type male and female mice developed more than 20% phosphorylated Rab10 ratios in serum, exceeding the measured pT73-Rab10 to total Rab10 ratio in all of the Tg-WT-BAC *Lrrk2* measured under basal conditions (Fig. 2F). The non-transgenic mice achieve this level of pT73-Rab10 phosphorylation despite expressing 10-fold lower levels of LRRK2 protein (0.21 ± 0.02 vs. 2.7 ± 0.16 ng/mL in the Tg-WT-BAC *Lrrk2* mice, males and females combined). These results show that LRRK2 protein is required, but not sufficient, for elevated extracellular pT73-Rab10 to total Rab10 ratios, and that wild-type mice can develop high levels (albeit variable) of phosphorylated Rab10 protein in serum.

Myeloid cells are well known to secrete small EVs as well as shed matrix proteins into the extracellular milieu to control immunological responses. Myeloid cells secrete proinflammatory EVs that include exosomes in response to immunological challenges, and both LRRK2 and Rab10 have been detected in extracellular protein fractions enriched in EVs [38]. Separation of a small panel of human serum ($n=3$ human serum samples) through a size-exclusion column optimized for serum separation of EVs from other extracellular compartments yielded three fractions that were characterized by whole-proteome analysis (Fig. 4G). The first elution, containing larger complexes, serum EVs and exosomes, shows the presence of peptides from canonical exosome proteins including CD9 (Fig. 4H). The pro-inflammatory myeloperoxidase protein, known to be upregulated with inflammation in myeloid cells and subsequently shed at high levels in both exosomes and non-EV serum fractions [39, 40], appears split in concentration between the first two elutions. Cytokines and chemokines of low molecular weight were present in the third elution (Fig. 4H). Similar to the distribution of myeloperoxidase, LRRK2 and pT73-Rab10 were both confined to fractions 1 and 2 from the column (Fig. 4I, J), whereas total Rab10 was also detected in fraction 3 (Fig. 4K). These results suggest that both LRRK2 and pT73-Rab10 may share a similar extracellular compartment in serum, enriched in EVs, but may not reside exclusively to exosomes.

The serum ratios of pT73-Rab10 to total Rab10 are elevated in *VPS35* and *SNCA* mutant mice

Recently, a pathogenic *VPS35* mutation, D620N, has been described to increase cellular levels of pT73-Rab10 in tissue lysates in a LRRK2-kinase dependent manner [41]. In serum samples procured from D620N-*VPS35* knockin mice, total LRRK2 and Rab10 protein concentrations are similar between littermate WT, heterozygous, and homozygous mice (Fig. 5A, B). In contrast, the ratio of pT73-Rab10 to total Rab10 is elevated in *VPS35*^{D620N/D620N} mice to $7.1 \pm 0.7\%$ (Fig. 5C), similar

to the average ratios in Tg-WT-BAC *Lrrk2* serum with over-expressed *Lrrk2* ($7.7 \pm 1.2\%$, Fig. 2F) as well as many of the septic wild-type mice (Fig. 4F). Analysis of whole blood from *VPS35*^{D620N/D620N} mice compared to wild-types shows the *VPS* mutant mice may have increased neutrophils and CD4-positive T cells, but similar numbers of monocytes (Fig. 5D-F). Western blot analysis of lysates derived from cultured bone-marrow derived macrophages (BMDMs) from the *VPS* mutant mice highlight the expected activating effects of the *VPS35* D620N mutation on increasing the normalized (to wild-type mice) ratio of pT73-Rab10 to total Rab10 (Fig. 5G). Interestingly, pT73-Rab10 was not reliably detected by either SiMOA or western blot in litter-mate wild-type mice from this strain processed at the same time. These results suggest that the *VPS35* mutation increases serum levels of the ratio of pT73-Rab10 to total Rab10 without affecting serum LRRK2 or total Rab10 levels.

We recently reported pathological α -synuclein aggregates may stimulate levels of pT73-Rab10 in a LRRK2-activity dependent manner in myeloid cells [12]. A transgenic mouse line expressing wild-type human α -synuclein (PAC-*SNCA*/*Snca*^{-/-} mice) harbors significant concentrations of α -synuclein aggregation and seeding activity according to past reports, accompanied by pronounced gastrointestinal disturbance phenotypes [42, 43]. In serum from these mice, both LRRK2 protein and total Rab10 is significantly increased compared to *Snca*^{-/-} control mice (Fig. 5H, I). The elevated ratio of pT73-Rab10 to total Rab at $5.1\% \pm 0.5$ in serum from these mice is higher than levels found in R1441C-*LRRK2* homozygous knockin mice (Fig. 5J). Flow cytometry analysis of whole blood from these mice demonstrates upregulated neutrophil populations, monocytes, as well as T-cells due to the *VPS35* mutation (Fig. 5K-M). However, different from the *VPS35* mutant mice, western blot analysis of isolated and cultured bone-marrow derived cells from the PAC-*SNCA*/*Snca*^{-/-} mice did not show intrinsically upregulated pT73-Rab10 levels compared to controls (Fig. 5N). Taken together, these data suggest that the extracellular ratios of pT73-Rab10 to total Rab10 in serum can be sensitive to genetic variants that stimulate LRRK2 activity (e.g., R1441C-*Lrrk2* or *VPS35* mutation), acute inflammation (e.g., sepsis), as well as chronic inflammation found in a progressive iPD α -synuclein transgenic model. Consistently, under basal conditions, serum pT73-Rab10 to total Rab10 ratios are very low in mice, undetectable in many cases. In all of these mouse cohorts evaluated at baseline, there were no differences observed between male and female mice from the same strain in serum LRRK2, Rab10, and pT73-Rab10 levels.

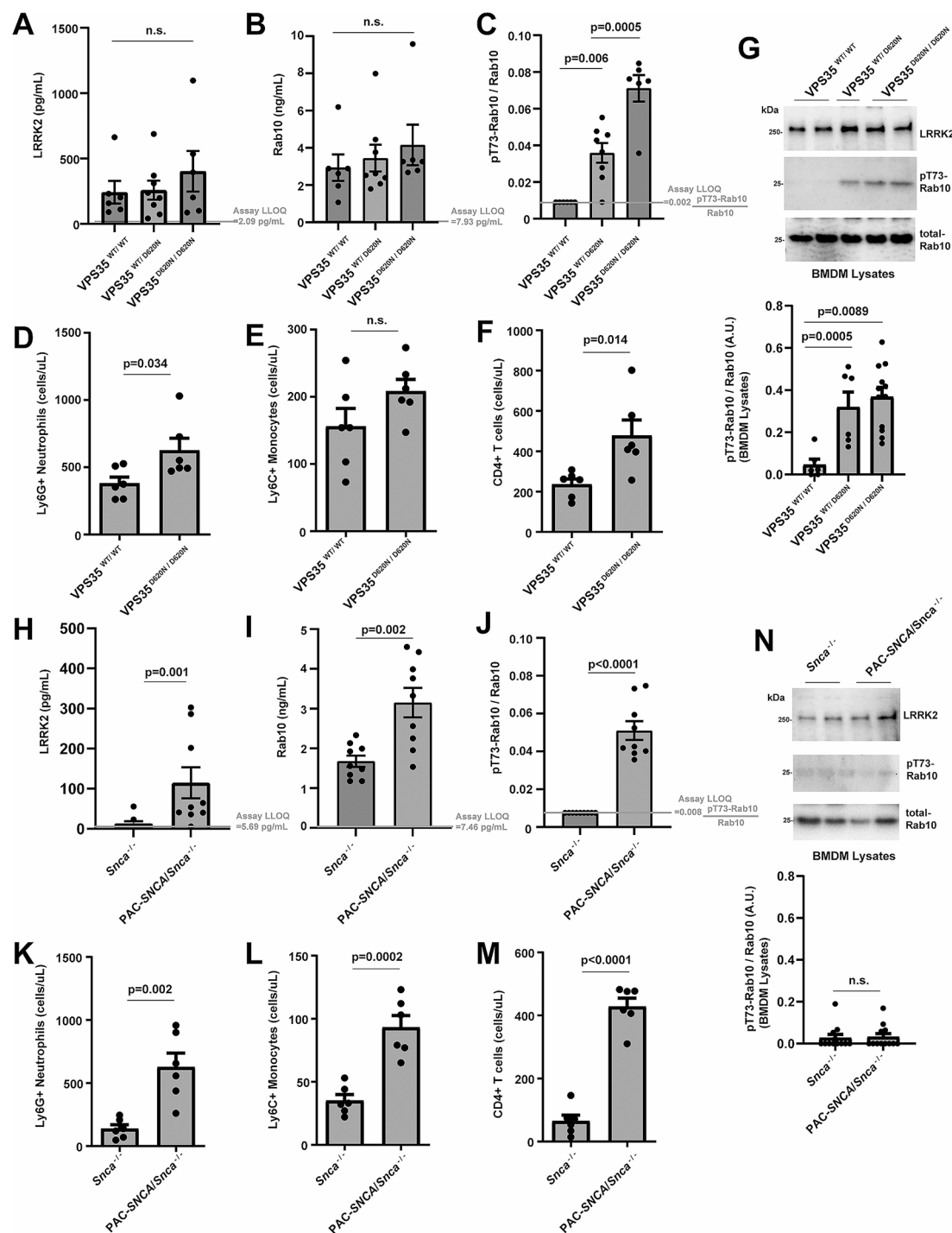


Fig. 5 The ratio of pT73-Rab10 to total Rab10 in serum is elevated in mouse models of late-onset PD. **(A)** Levels of total LRRK2, **(B)** total Rab10 and **(C)** the ratio of pT73-Rab10 to total Rab10 as measured by SiMOA in venous serum from *VPS35^{WT/WT}* (2 males and 4 females) mice, *VPS35^{WT/D620N}* (4 males and 4 females) mice, and *VPS35^{D620N/D620N}* (6 males) mice. **(D)** Graphs show numbers of neutrophils (CD11b+Ly6G+), **(E)** classical monocytes (CD11b+Ly6G-Ly6C+), and **(F)** CD4 T-cells measured by flow cytometry in *VPS35^{WT/WT}* and *VPS35^{D620N/D620N}* serum samples. **(G)** Representative immunoblots and quantification of cultured bone marrow derived macrophages demonstrating elevated pT73-Rab10 to total Rab10 levels with mutant *VPS35* expression. **(H)** Levels of total LRRK2, **(I)** total Rab10 and **(J)** the ratio of pT73-Rab10 to total Rab10 from *Snca^{-/-}* (3 males and 6 females) mice, and *PAC-SNCA/Snca^{-/-}* (5 males and 4 females) mice. **(K)** Graphs show numbers of neutrophils (CD11b+Ly6G+), **(L)** classical monocytes (CD11b+Ly6G-Ly6C+), and **(M)** CD4 T-cells measured by flow cytometry in *Snca^{-/-}* and *PAC-SNCA/Snca^{-/-}* mice blood. **(N)** Representative immunoblots and quantification of cultured bone marrow-derived macrophages demonstrating low but equivalent pT73-Rab10 to total Rab10 between *Snca^{-/-}* and *PAC-SNCA/Snca^{-/-}* mice. Mouse ages ranged from 3–6 months. Columns depict group mean, dots represent the mean values from an animal or independent experiment, and error bars show SEM. P values are from two-tailed t-tests or one-way ANOVA analysis with Tukey's multiple comparison when three groups are tested

The ratio of pT73-Rab10 to total Rab10 in serum is pharmacodynamic

Cellular levels of pT73-Rab10 are known to be highly pharmacodynamic and drop within minutes of LRRK2 kinase inhibition [44], but the extracellular ratio of pT73-Rab10 to total Rab10 has not been previously measured in response to drugs. The small molecule LRRK2 inhibitor PFE-360 is orally available and quickly metabolized in mice and rats, with a serum half-life in oral dosing of $t_{1/2} = \sim 1.3$ h in rats and a potency of $\sim IC_{50}$ 6 nM in vitro for LRRK2 kinase inhibition [45]. To determine the pharmacodynamic potential of the extracellular ratio of pT73-Rab10 to total Rab10 in serum, we produced longitudinal sets of serum samples from rodent strains with elevated

pT73-Rab10 levels, including Tg-G2019S-BAC *Lrrk2* and *VPS35* mutant mice, treated with a single dose (10 mg per kg) of PFE-360. Measured serum levels of the ratio of pT73-Rab10 to total Rab10 become depressed within 30 min of the oral gavage of drug in both strains of mice (Fig. 6A, B). Still lower levels were recorded at one-hour post dose, 78.3 \pm 9.1% inhibition in *VPS35* knockin mice and 83.3 \pm 7.4% inhibition in Tg-G2019S-BAC *Lrrk2* mice. In the facial vein collections of serum, when insufficient volume or a hemolyzed blood sample was collected, the sample was omitted from analysis and collection attempted again at the next time point (Fig. 6A-C). At the one-hour post-drug treatment time point in wild-type rats, serum levels of the ratio of pT73-Rab10 to total

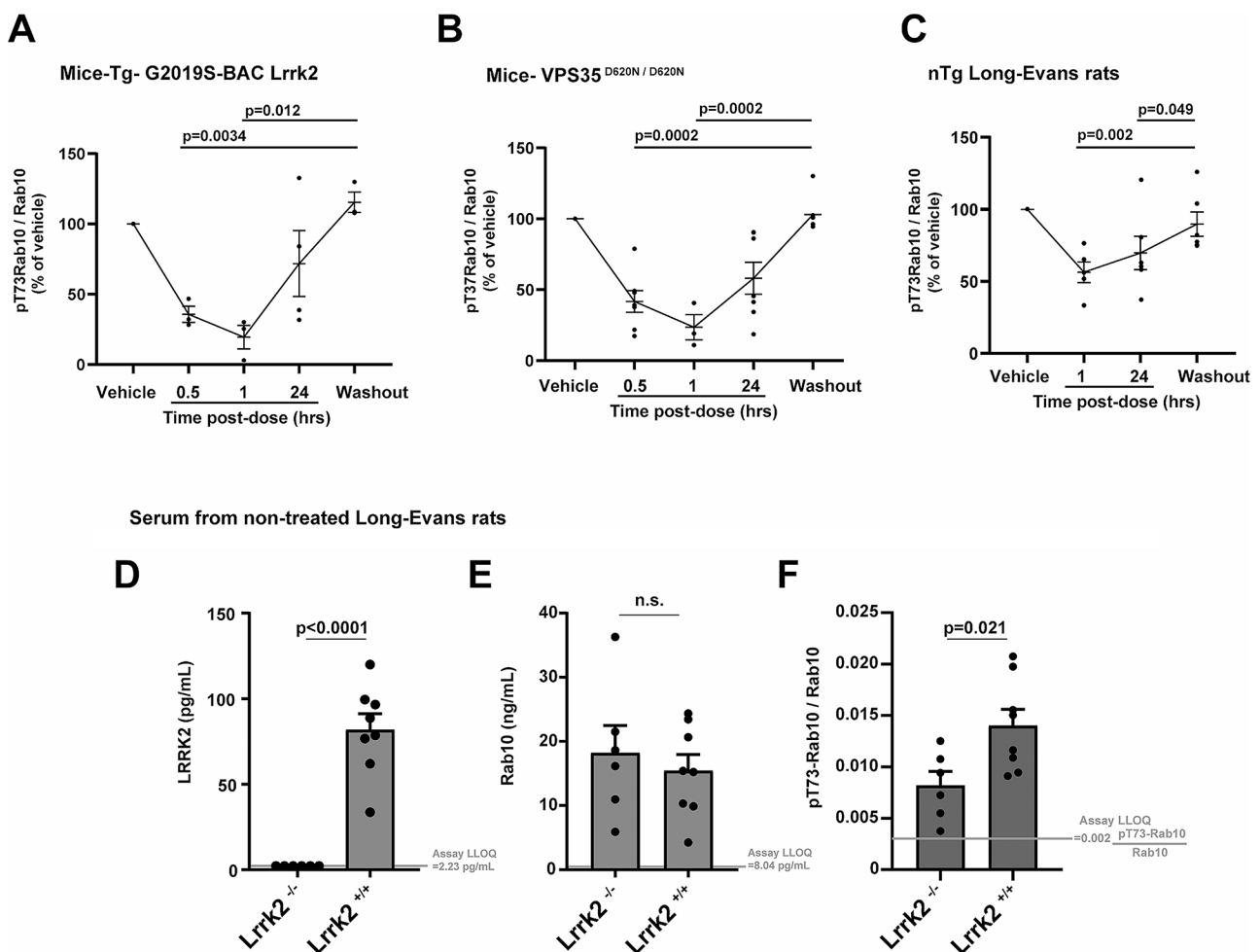


Fig. 6 The ratio of pT73-Rab10 to total Rab10 in serum is pharmacodynamic. In mice and rats, the LRRK2 small molecule inhibitor PFE-360 was given as a single oral dose (10 mg per kg), serum (mouse facial vein or rat lateral saphenous vein) collected one-hour after a vehicle-only administration (Vehicle), and serum next collected at the indicated time post-drug administration, with a final collection at 48 h after drug (Washout). The ratio of pT73-Rab10 to total Rab10 diminishes relative to baseline in (A) Tg-G2019S-BAC-*Lrrk2* (4 male mice) and (B) *VPS35*^{D620N/D620N} (7 male mice), as well as (C) nTg Long-Evans *Lrrk2*^{+/+} rats (7 male rats). Rodent ages were 3–5 months, bars show group means, error bars show SEM, and dots show the mean values from individual rodents. In repetitive venous draws, some samples were not successfully collected due to insufficient volume collected or hemolysis, thereby excluding the sample for analysis (see Additional File S3 for all raw data collected). Bars in panels A-C show group mean, error bars show SEM, and p values were calculated from one-way ANOVA analysis with Tukey's post-hoc comparisons. (D) Graphs show levels of LRRK2, (E) Rab10, and (F) the ratio of pT73-Rab10 to total Rab10 in Long-Evans *Lrrk2*^{-/-} rats (3 males and 3 females) compared to non-transgenic Long-Evans *Lrrk2*^{+/+} rats (4 males and 4 females). Columns in panels D-E show group mean, error bars show SEM, and p values are from two-tailed t-test

Rab10 were only $37.4 \pm 8.3\%$ lower compared to baseline levels, with continued suppression evident 24 h post-gavage (Fig. 6C).

To pinpoint why only a minority of pT73-Rab10 was inhibited in the wild-type rats, we generated another set of serum samples from a new cohort of wild-type (Long Evans outbred) rats together with serum from *Lrrk2*^{-/-} rats (also Longs Evans background), with the knockout rat serum representing the lowest ratio of pT73-Rab10 to total Rab10 attributable to LRRK2. As anticipated, there were no measurable quantities of LRRK2 protein in serum from *Lrrk2*^{-/-} rats (Fig. 6D). Serum levels of total Rab10 were similar between the wild-type and knockout strains (Fig. 6E). However, the ratio of pT73-Rab10 to total Rab10 was only partially lowered in the *Lrrk2*^{-/-} rats compared to wild-types. The reduced level in the knockout rats was similar to the reduction measured one hour after PFE-360 gavage ($41.1 \pm 8.7\%$ reduction in the knockout compared to $37.4 \pm 8.2\%$ reduction with PFE-360). These results suggest that serum pT73-Rab10 levels in rats, which are low to begin with (all rat samples measured $< 2.5\%$ pT73-Rab10 to total Rab10), are only partially dependent on LRRK2 under basal conditions.

Ratios of pT73-Rab10 to total Rab10 are elevated in PD cases with higher MDS-UPDRS scores

To better understand the ratio of pT73-Rab10 to total Rab10 in the periphery in iPD, we selected a cohort of serum samples donated from participants enrolled in the Parkinson's Disease Biomarker Program (PDBP). 522 serum samples were available from 276 PD cases and 246 controls originating from a single collection site (Table 1). Serum samples matched whole-blood transcriptomic and genetic data generated from participant tubes of blood collected at the same time as the serum samples, and all clinical and demographic data were collected during the same visit as the blood tube collections. Blood draws occurred between the hours of 8 and 10 in the morning, with all participants taking their normal routine of medications. L-dopa equivalent daily dosages (LEDD) at the time of sample donation were calculated. Clinical and demographic characteristics in the cohort highlight lower UPSIT scores in the PD group, reflecting hyposmia in some cases, and nominally worse cognition reflected in lower MoCA scores (Table 1). The PD and control group had a similar usage of anti-inflammatories (NSAIDs) and statins. LEDDs are moderately correlated to motor defects reflected in MDS-UPDRS part III scores ($r=0.44$, $p<0.0001$).

SiMOA measurements of total LRRK2, total Rab10, and pT73-Rab10 in human sera were made without respect to group assignment in a randomized fashion from coded samples. Analysis of assay performance across the cohort shows a dynamic linear range of ~2–3

orders of magnitude in sensitivity in each run, consistent lower limits of quantification (LLOQ) from run-to-run, and low variability (coefficient of variations) across technical replicates (Supplemental Fig. S2). Similar to studies in rodents, ~60 μ l of serum were utilized for measurements of all three analytes with technical replicates. In addition to LRRK2, total Rab10, and pT73-Rab10, serum creatinine values were measured in the same samples by ELISA. Creatinine levels for all samples fell within normal ranges and did not correlate with total LRRK2 levels ($r=-0.017$, $p=0.70$), total Rab10 ($r=0.069$, $p=0.12$), pT73-Rab10 levels ($r=0.024$, $p=0.58$), or the ratio of pT73-Rab10 to total Rab10 ($r=0.065$, $p=0.14$). All samples were estimated to have hemoglobin concentrations less than 100 mg per dL using standard scales and none of these were excluded based on hemolysis. Twenty serum samples, selected at random, were analyzed for exact hemoglobin values via ELISA analysis, and no correlations were found between hemoglobin levels and any of the other proteins measured. Further, no correlations were found between LRRK2, total Rab10, or pT73-Rab10 and freezer storage time.

In the analysis of total LRRK2 protein, mean values of LRRK2 at 6,537 pg per mL (95% C.I. [1,501 to 11,573]) across all human samples were, on average, much higher than those observed in serum from mice (111 ± 17 pg per mL [SEM]) and rats (82 ± 6 pg per mL [SEM]). However, the Tg-*Lrrk2* BAC mice (mean of both WT and G2019S strains) had LRRK2 expression ($3,460 \pm 265$ pg per mL [SEM]) closer to that found in humans. These results may be consistent with observations from western blots we previously performed from macrophage cell lysates, where LRRK2 protein levels were similar between BAC strains and human primary macrophages, and much lower in macrophages from non-transgenic mice, irrespective of interferon stimulation [12].

Male PD subjects had slightly higher LRRK2 expression than female controls, with an average difference of 0.96 ng per mL (95% C.I. [0.26 to 1.65], adjusted $p=0.003$, Supplemental Fig. S3). However, a least squares multivariate regression approach did not reveal any significant associations between LRRK2 levels in serum and clinical rating scales including MDS-UPDRS scores, MoCA, UPSIT, and Epworth Sleep scales, with all clinical scales recorded within hours of the serum sample donation with patients taking their normal routine of medication. Across the cohort, total Rab10 levels are also much higher in the average human serum sample (mean 78 ng per mL, 95% C.I. [56 to 100]) compared to the average serum sample from non-transgenic mice (4 ± 0.5 ng per mL [SEM]) and Long-Evans rats (15 ± 3 ng per mL [SEM]). Despite successful measurements of total LRRK2 and total Rab10 levels in all samples in the 522-sample cohort, a sizable proportion of samples (23.5%) had levels of pT73-Rab10

below the empirically determined average assay lower limit of quantification (LLOQ, 10.1 pg of pT73-Rab10 per mL, Supplemental Fig. S3). To prevent the assignment of a null value for the ratio of pT73-Rab10 to total Rab10 for these samples and exclusion from further statistical analysis, the LLOQ for pT73-Rab10 was divided by the measured total Rab10 in the sample to obtain an overestimated numerical ratio for pT73-Rab10 to total Rab10. Because total Rab10 tends to be high in all human serum samples, the ratio value of pT73-Rab10 to total Rab10 in these samples remained very low, with a mean ratio of 0.0036 for pT73-Rab10 to total Rab10, 95% C.I. [0.0030 to 0.0042]. This low level of phosphorylation can be considered biologically insignificant, similar to those determined in *Lrrk2*^{-/-} mice with this method.

In rodents, the highest recorded ratio of pT73-Rab10 to total Rab10 was 38.2%, found in a serum sample from a male Tg-G2019S-BAC *Lrrk2* mouse. While many human serum samples had very low pT73-Rab10 levels, comparable to levels observed in wild-type mice and rats under basal conditions, a sizable proportion of human serum samples (9.8%, or 51 of 522 samples) had ratio values that exceeded 38.2% (i.e., the highest recorded value observed in transgenic mice). Two of the 522 samples (0.4% of total samples) had a ratio of pT73-Rab10 to total Rab10 above 1.0, specifically, 1.25 and 1.27, likely reflecting inaccuracy associated with the regression of the assay at the highest ends of the measures. Both these samples (2 of 522) were adjusted to ratio values of 1.0 that represent the upper limit of the assay. The ratio of pT73-Rab10 to total Rab10 was variable across the cohort, and efforts to improve normalcy of the distribution with additional transformations were not successful, owing to both the very high and very low values within the constrained measures (Supplemental Fig. S3). Distributions of the ratio of pT73-Rab10 to total Rab10 were overall similar between participants with and without PD (Supplemental Fig. S3). Within the cohort of samples, two control subjects donated serum weekly across a two-month interval. LRRK2 serum levels and the ratio of pT73-Rab10 to total Rab10 were relatively stable over this time period, with one subject consistently showing higher LRRK2 and pT73-Rab10 to total Rab10 ratios than the other subject (Supplemental Fig. S4).

In samples across the cohort, serum LRRK2 protein levels strongly correlate with serum total Rab10, pT73-Rab10, and the ratio of pT73-Rab10 to total Rab10 (Fig. 7A-C). A stepwise regression analysis including all demographic and clinical variables listed in Table 1, as well as LRRK2 genotypes G2019S, rs76904798, N2081D, as well as N551K/R1398H, found that MDS-UPDRS scores, as well as the G2019S-*LRRK2* mutation and total LRRK2 levels significantly predicted the ratio of pT73-Rab10 to total Rab10. In a least squares model (RMSE=0.20, $r=0.33$, $p<0.0001$) that includes

MDS-UPDRS part III scores, G2019S-*LRRK2* mutation status, and LRRK2 levels in serum, a doubling of LRRK2 serum levels is associated with an increase of 1.4% of pT73-Rab10 to total Rab10 (95% C.I. [0.40–0.24%], $p=0.0063$). An increase of a point on the MDS-UPDRS part III scale is associated with an increase of 0.28% pT73-Rab10 to total Rab10 (95% C.I. [0.089–0.47%], $p=0.0043$). Finally, the presence of the G2019S mutation is associated with a larger increase of 19.0% pT73-Rab10 to total Rab10 (95% C.I. [8.99–29.0%], $p=0.0002$). Other variables in the model including age, sex, disease duration, L-dopa equivalent daily dose (LEDD), and current usage of non-steroidal anti-inflammatories (NSAIDs), did not significantly predict the ratio of pT73-Rab10 to total Rab10.

While only four subjects in the cohort had a G2019S-*LRRK2* heterozygous mutation, all four had a very high measured serum ratio of pT73-Rab10 to total Rab10 (mean value $52.1 \pm 16.9\%$ [SEM]). As the G2019S-*LRRK2* mutation is considered pathogenic in PD cases, a rough initial estimation of a pathogenic level of Rab phosphorylation may be represented through the average ratios found in the mutation carriers, or ~50% pT73-Rab10 to total Rab10. A stratum of iPD cases without *LRRK2* mutations demonstrated this level or above of pT73-Rab10 to total Rab10. Splitting the PD cases in the cohort between participants with high (e.g., pathogenic levels) ratios that exceed 50% from those with levels less than 50% highlights worse MDS-UPDRS part III scores in PD cases with higher Rab10 phosphorylation (Fig. 7D). The high pT73-Rab10 group of PD patients is 7.3 points worse on the MDS-UPDRS part III score than those with lower Rab phosphorylation ($p=0.012$, Mann Whitney U test). The difference of 7.3 points on the MDS-UPDRS part III is associated with approximately three years of disease progression in iPD [46], but there is a similar disease duration between the high and low pT73-Rab10 groups (~8 years on average, Fig. 7D), and there is no correlation between disease duration and the ratio of pT73-Rab10 to total Rab10 across the cohort ($r=-0.006$, $p=0.92$). Splitting the cohort according to PD diagnosis, NSAID use, or sex, did not reveal any group differences in ratios of pT73-Rab10 to total Rab10 (Supplemental Fig. S5). These results suggest that PD cases with higher pT73-Rab10 to total Rab10 ratios have worse motor impairment, irrespective of disease duration.

Elevated pT73-Rab10 to total Rab10 ratios in human serum are associated with antigenic pro-inflammatory responses in innate immune cells

Together with the serum samples, a second tube of whole blood was collected into PAXgene blood RNA tubes (IVD) for whole-transcriptomic analysis. Across the samples, *LRRK2* mRNA in whole blood is significantly but

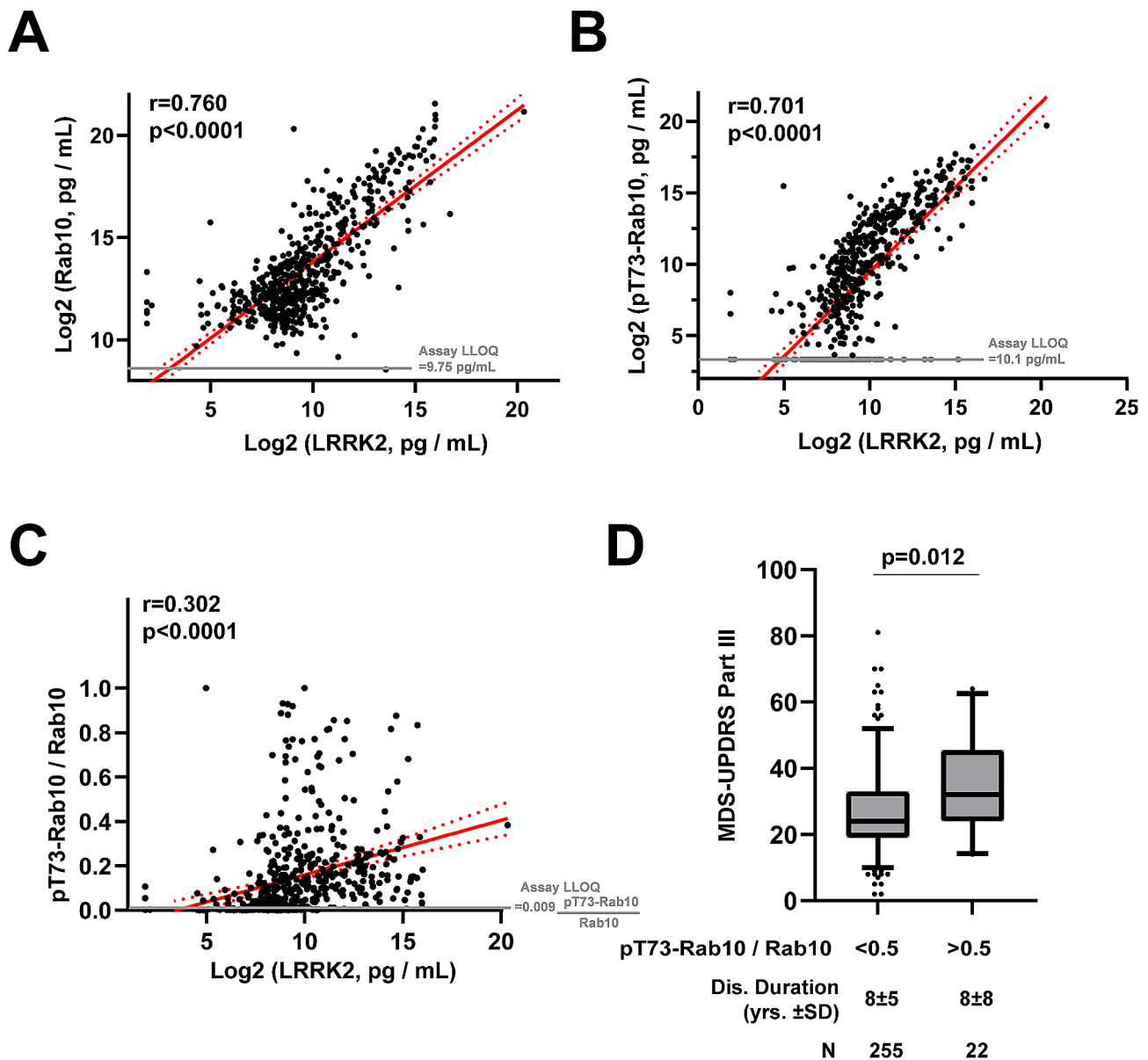


Fig. 7 LRRK2 protein levels predict pT73-Rab10 levels that are elevated in PD cases with worse MDS-UPDRS scores. **(A)** Scatter plots show relationships between measured serum levels of total Rab10 and LRRK2, **(B)** pT73-Rab10 and LRRK2, and **(C)** the ratio of pT73-Rab10 to Rab10 and LRRK2. $N=522$ cases and controls (see Table 1). R values show correlation coefficients and p values correspond to mean linear regression analysis of lines (red) with 95% confidence intervals shown (red dashed curves). **(D)** Box and whisker plot comparing the mean MDS-UPDRS part III scores in PD cases split to lower (<0.5) and higher (>0.5) ratios of pT73-Rab10/Rab10. P value indicated is from a Mann-Whitney U test for comparisons of groups with unequal sizes

weakly correlated with LRRK2 protein levels in serum ($r=0.119$, $p=0.007$), but not correlated at all to the ratio of pT73-Rab10 to total Rab10 ($r=0.008$, $p=0.848$). Therefore, *LRRK2* mRNA cannot be used to predict LRRK2-directed Rab10 phosphorylation. To identify other genes and gene networks that might correlate with the ratio of p773-Rab10 to total Rab10 better, a weighted gene co-expression network analysis (WGCNA) identifies two gene modules in association (Fig. 8A). The Purple gene module positively correlates with the ratio of pT73-Rab10 to total Rab10 as well as MDS-UPDRS III scores

and LRRK2 levels in serum. The top-ranked cluster of interacting proteins encoded within the Purple module, identified by K-means clustering (mean local clustering coefficient 0.81, and Supplemental Fig. S6), highlights upregulated antigen presentation genes including *HLA-B*, *HLA-C*, and *HLA-E* (Fig. 8B). Notably, variation in the *HLA-C* locus associates with PD-risk in genome-wide studies [47]. Differential gene expression analysis (DEG) demonstrates that mRNAs of several genes in the top-ranked Purple protein cluster (Fig. 8B) are upregulated in PD blood including *TYROBP* (\log_2 FoldChange=0.22,

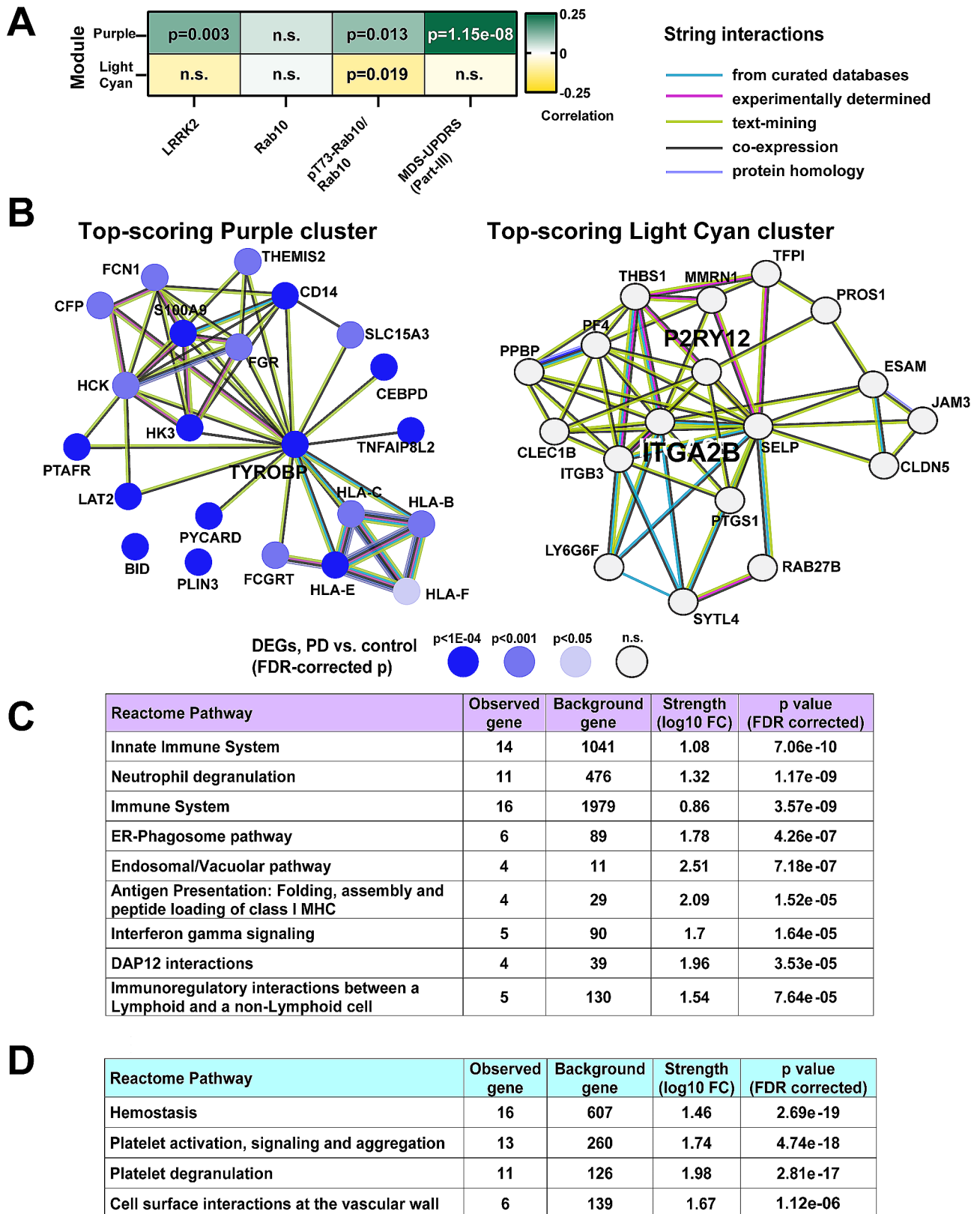


Fig. 8 (See legend on next page.)

(See figure on previous page.)

Fig. 8 The ratio of pT73-Rab10 to total Rab10 in serum, and MDS-UPDRS III scores, are associated with myeloid cell activation and antigenic responses. **(A)** A weighted gene co-expression network analysis (WGCNA) identifies 27 gene modules of densely co-expressed genes (see Supplemental Fig. S6 for hierarchical clustering). Two modules, Purple and Light Cyan, are significantly correlated with the ratio of pT73-Rab10 to total Rab10. Pearson's correlation coefficients and associated p values are additionally shown for correlation to LRRK2 protein levels in serum and MDS-UPDRS-III scores. **(B)** Top-scoring StringDB protein-protein interaction clusters from Purple and Light Cyan modules are shown. Differentially expressed genes (DEGs) in PD subjects vs. control are indicated from DESeq2 negative binomial fit, with level of significance (Benjamini-Hochberg adjusted p values) shown with a blue gradient. **(C)** All terms from the Reactome Pathway database (FDR-corrected p-value cutoff 1×10^{-4}) are listed. Top process terms from Purple ($N = 290$ searchable genes) and **(D)** Light Cyan ($N = 102$ searchable genes) are shown. All terms with a $p < 0.05$ cutoff from multiple databases are listed in Supplemental Material 3

Benjamini-Hochberg corrected $p = 5.07 \times 10^{-6}$) and *CD14* ($\log_2\text{FoldChange} = 0.23$, Benjamini-Hochberg corrected $p = 6.56 \times 10^{-5}$). Other proteins in the Purple module cluster include CD14, a canonical surface marker for myeloid cells and coreceptor for toll-like receptors (TLRs), and the immunoreceptor tyrosine-based activation motif (ITAM), TYROBP, that regulates triggering receptor expressed on myeloid cells 2 protein (TREM2). In contrast to the Purple module, the ratio of pT73-Rab10 to total Rab10 is negatively correlated with the expression of genes in the Light Cyan module. The cluster of genes co-expressed in the Light Cyan module (mean local clustering coefficient = 0.808) highlights platelet integrin ITGA2B that connects to the platelet glycoprotein GP9, and interacts with P2RY12, a protein also associated with homeostasis in microglia. The Light Cyan cluster of genes are all highly expressed in platelets in blood and play central roles in immune interactions at the vascular wall (Fig. 8D). However, none of the Light Cyan cluster genes are differentially expressed between PD and controls in this cohort.

Discussion

The relationship between LRRK2-mediated Rab phosphorylation and disease progression has been poorly understood, in part due to the lack of sensitive and specific assays to evaluate these proteins that are low in concentration in most cells and biofluids. In different models, the LRRK2 substrate Rab10 has been implicated in immune functions related to both infection and PD [7, 9, 10, 12, 21]. As LRRK2 interacts with Rab proteins on vesicles, and some of these vesicles shed into the extracellular space, we utilized recent developments in single-molecule assay technology to design ultrasensitive assays to measure extracellular ratios of pT73-Rab10 to total Rab10. This is the first study we are aware of to evaluate hundreds of cases and controls for Rab phosphorylation, and a number of observations could be made in both rodent models and human samples. The ratio of pT73-Rab10 to total Rab10, as measured in biobanked serum samples, is highly dynamic and can rapidly diminish with oral administration of a LRRK2 inhibitor. These results may be compatible with evidence that extracellular vesicles and other components in serum shed from immune cells in blood may have very short half-lives, for example ~ seven minutes in mice for exosome proteins [48]. In

past studies in mice and rats, measures of LRRK2 kinase activity have typically required sacrificing the animal for western blot assessments of tissues, or procurement of cells from large volumes of blood. Since measurements from all three assays, total Rab10 and LRRK2, and pT73-Rab10, are accomplished with less than ~ 60 μl of serum, routine longitudinal measures in both clinical and rodent model samples are now possible.

Specificity of the assays is incredibly important in understanding the underlying biology of LRRK2 activity changes in different disease states and progression. The observed strong correlation between extracellular LRRK2 protein levels and pT73-Rab10 protein levels in serum across the cohort ($r = 0.70$, $p < 0.0001$) implies that most phosphorylated Rab10 in human serum is LRRK2-activity related. Evaluation of serum from clinical trial samples of LRRK2 kinase inhibitors will be informative to determine if all pT73-Rab10 signal from human sera is LRRK2-activity dependent, as it appears to be in the mouse models used in this study. Previous studies with clinical samples from LRRK2 inhibitor trials did not incorporate measures of the ratio of pT73-Rab10 to total Rab10 [49, 50], so it is difficult at present to compare our results in serum to other studies using different sources of protein. Following, a caveat to the interpretation of past studies is that the lack of total Rab10 measures to normalize the pT73-Rab10 levels may conflate lower total Rab10 levels with a reduction in LRRK2 kinase activity. For example, a diminished level of total Rab10 in serum, such as through immune cell depletion or that we observed in sepsis, may not necessarily reflect diminished LRRK2 activity should the ratio of pT73-Rab10 to total Rab10 persist at normal levels. In the human cohort of samples, total Rab10 protein levels positively correlate with pT73-Rab10 levels (in PD cases and controls, $r = 0.61$, $p < 0.0001$). Therefore, higher total Rab10 levels may erroneously drive the appearance of higher LRRK2 activity if only pT73-Rab10 is measured without an analysis of total Rab10. Our data suggest initial prioritization of the ratio of pT73-Rab10 to total Rab10 as a truer metric of LRRK2 activity, since LRRK2 expression or activity does not appear to influence total Rab10 levels, though total Rab10 would also be expected to have biology independent of LRRK2 that may be reflected in secreted levels. Notably, the associated protocols used here are made available online via Protocols.io in graphical step-by-step formats (see Methods),

with commercially available parts and reagents. We expect the foundational results reported here together with the new assays will lead to a better understanding of how LRRK2 activity-dependent changes in the periphery may wax and wane in different disease models, and correlate with phenotypes in the brain. Samples already biobanked as part of ongoing clinical trials can also be rapidly assessed, as we have not observed significant freezer storage time effects on pT73-Rab10 levels. Other variables such as freeze thaw stability, performance across sites, and lot-to-lot performance characteristics with different lots of antibodies remain to be assessed. Further, assay characteristics in plasma remain to be determined, though we expect similar outstanding characteristics as other commercial assays based on this platform perform well in multiple fluid compartments from blood.

Another important result from this study is that iPD patients with a very high ratio of pT73-Rab10 to total Rab10 in serum demonstrate worse clinical scores on the MDS-UPDRS III scale, as well as blood transcriptomic profiles that suggest elevated neutrophil and antigenic responses, compared to other iPD cases. This result should be replicated in additional cohorts to build a higher confidence of the novel relationships disclosed here, as well as in well-phenotype longitudinal cohorts. In this cohort, the ratio of pT73-Rab10 to total Rab10 significantly (albeit weakly) predicts the expression of multiple *HLA* genes, including *HLA-C* that harbors variants associated with iPD risk [47]. Whether LRRK2 kinase activity and Rab phosphorylation modifies HLA traffic and antigen presentation in myeloid cells, or is responsive to these changes through the process of immune cell maturation, is an area of ongoing investigation [51]. Though it is unclear whether LRRK2 activity itself is modifying peripheral innate-immune cell inflammation, or responsive to it, it seems clear that there were no anti-inflammatory medications used by the participants in this study that appeared effective in reducing pT73-Rab10 levels. The reason for very high pT73-Rab10 levels found in some iPD patients is not known, and will be difficult to definitively pinpoint without intervention. In a recent study, we identified α -synuclein aggregates as a potent stimulator of pT73-Rab10 in monocytes, microglia and macrophages [12]. A critical clue in the mouse models studied here could be the high levels of pT73-Rab10 recorded in the serum of mice expressing wild-type *SNCA* at physiologically relevant levels [12, 42, 43]. We hypothesize that the high pT73-Rab10 signatures in some *LRRK2*-negative iPD cases may be due to extensive and progressive peripheral and central α -synucleinopathy, further modified by the PD-linked gut microbiome. Combining α -synuclein seeding assays and gut microbiome analysis in peripheral samples, serum, and CSF

with LRRK2 activity biomarkers like pT73-Rab10 may help identify possible associations between these disease-associated features.

G2019S-*LRRK2* mutation carriers are known to have a more benign progressive motor phenotype over the course of disease compared to iPD cases [2]. Here, *LRRK2*-negative iPD carriers that show pT73-Rab10 levels in serum just as high (or above) that found in G2019S-*LRRK2* carriers have worse motor scores than other iPD cases with lower pT73-Rab10 levels. We can speculate on several potential explanations for these seemingly paradoxical observations. It can be presumed that the cause of upregulated pT73-Rab10 in *LRRK2*-negative iPD is fundamentally different from the cause of high pT73-Rab10 in G2019S-*LRRK2* carriers. The difference is exemplified in the mouse studies here showing that some septic wild-type mice developed similar pT73-Rab10 levels (or higher) than transgenic G2019S-*LRRK2* mice, and most wild-type septic mice showed higher serum pT73-Rab10 levels than R1441C-*Lrrk2* knockin mice. Though we did not perform behavioral evaluations of mice in this study, the septic mice are clearly sicker than transgenic G2019S-*LRRK2* mice, as expected, because the cause of elevated pT73-Rab10 is different, even though inflammation may be central to both genetic and environmental factors that stimulate pT73-Rab10. Thus, elevated pT73-Rab10 in *LRRK2*-negative iPD may reflect a different but nevertheless detrimental disease process than that occurring in G2019S-*LRRK2* carriers. For example, recent studies show that many G2019S-*LRRK2* carriers are α -synuclein negative according to seeded-aggregation assays, with rarified α -synuclein pathology in the brain [52, 53]. Since α -synuclein aggregates can drive pT73-Rab10 levels in immune cells [12], the difference in α -synuclein pathological progression between G2019S-*LRRK2* mutation carriers and iPD may impact disease-related endpoints, even if pT73-Rab10 levels are comparable.

Recent data suggests the G2019S-*LRRK2* mutation in patients increases the secretion of bis(monoacylglycerol) phosphate (BMP) in urine [54], with BMP primarily localized to late endosomal and lysosomal membranes [55]. In macrophages, pT73-Rab10 likewise localizes primarily to late endosomal and lysosomal membranes [7]. Given that the effects of the G2019S-*LRRK2* mutation on phosphorylated Rabs have been difficult to resolve in cellular lysates [16, 17, 21], when expression of G2019S-*LRRK2* is matched to WT-*LRRK2*, it seems possible that G2019S-*LRRK2* may increase the export of pT73-Rab10 protein to the extracellular space, similar to BMP glycerophospholipids. Additionally, a study using a pull-down mass-spectrometry based approach demonstrated that the G2019S-*LRRK2* mutation increases LRRK2 protein in CSF [56]. Since the routine analysis of cellular lysates does not typically account for the abundance of

extracellular proteins, we propose that the effects of the *G2019S-LRRK2* mutation may be apparent more readily in the analysis of biofluids that may harbor increased BMP, LRRK2 protein, and phosphorylated Rab proteins like pT73-Rab10. Future studies well-powered for *G2019S-LRRK2* mutation status that measure all of these markers, from both PD cases and non-manifesting carriers, will be informative in this regard.

Fluid biomarkers in neurodegenerative diseases continue to have a transformative effect on understanding disease progression. Assays for proteins reflecting pathology including neurofilament light chain (NFL [57]), phosphorylated tau (e.g., pTau-181 [58]), and α -synuclein (both exosome-based [59] and seeding [60]), are now widely utilized in pre-clinical and clinical research. In contrast, much less is known about the biochemical activity associated with risk factors in iPD that include LRRK2 and glucocerebrosidase. While measures of phosphorylated Rab proteins or glucocerebrosidase activity are unlikely to be diagnostic for PD, they may provide critical information on how these activities change in disease, what drives these changes, and how best to therapeutically intervene.

Conclusions

These data identify elevated LRRK2 kinase activity in the periphery, reflected in accurate measures of the ratio of pT73-Rab10 to total Rab10, as a biomarker for exacerbated inflammation. The type of inflammation associated with pT73-Rab10 to total Rab10 ratios, antigenic neutrophil responses, correlates with worsened disease endpoints in iPD. The assays provided here, ready for deployment in many laboratories and clinical sites across neurodegeneration research, will facilitate the discovery and advancement of new and effective LRRK2-targeting treatments to potentially help identify the patients most likely to benefit.

Abbreviations

PD	Parkinson's disease
LRRK2	Leucine-rich Repeat Kinase 2
VPS35	vacuolar protein sorting 35
PBMC	peripheral-blood mononuclear cells
NFL	Neurofilament Light Chain
SiMOA	Single Molecule Assay
SDS	Sodium Dodecyl Sulfate
SNCA	Synuclein- Alpha
IFN γ	Interferon Gamma
TNF	Tumor Necrosis Factor
PDBP	Parkinson's Disease Biomarker Program
AMP-PD	The Accelerating Medicines Partnership Parkinson's Disease programme
DMR	Data Management Resource
MDS-UPDRS	Movement Disorders Society-Unified Parkinson's Disease Rating Scale, part I-IV
MoCA	The Montreal Cognitive Assessment
UPSIT	University of Pennsylvania Smell Identification Test
LEDD	L-dopa Equivalent Daily Dosage
SD	Standard Deviation

SEM	Standard Error Of The Mean
IQR	Interquartile Range
CI	Confidence Interval
LL	Lower Limit Of Confidence Interval
UL	Upper Limit Of Confidence Interval
BMDM	Bone Marrow-Derived Macrophage

Supplementary Information

The online version contains supplementary material available at <https://doi.org/10.1186/s13024-024-00738-4>.

Supplementary Material 1

Supplementary Material 2

Supplementary Material 3

Acknowledgements

Not applicable.

Author contributions

Y.Y., H.L., K.S., T.M., A.C., N.B., S.S., M.E., and R.B. performed experiments, analyzed data, and wrote the manuscript. L.H.S., M.W.L., D. V., and A.B.W. analyzed data and wrote the manuscript. T.A.Y., D.G.S., and D.J.M., contributed critical tools and wrote the manuscript. All authors read and approved the final manuscript.

Funding

This study was supported by NIH R01 NS064934, NIH P50 NS108675, NIH R01 NS119528, NIH R01 NS105432, and The Michael J. Fox Foundation (MJFF) for Parkinson's Disease Research (MJFF-022434).

Data availability

Raw data are available for download online in Supplemental Material 1.

Declarations

Ethics approval and consent to participate

All study protocols were approved by local Institutional Review Boards at the University of Alabama at Birmingham and Duke University, and Institutional Animal Care and Use Committees at Duke University and the Van Andel Institute.

Consent for publication

Not applicable.

Competing interests

A.B.W. has served as a member of The Michael J. Fox Executive Foundation (MJFF) Scientific Advisory Board and is a paid consultant for SciNeuro, Inc, and has been a paid consultant for EscapeBio Inc; and has received research grants from Biogen Inc. and EscapeBio, Inc., as well as MJFF, ASAP Foundation, Parkinson's Foundation, and the National Institutes of Health (NIH). A.B.W. is part owner of a series of LRRK2 kinase inhibitors (WO 2013166276) and part owner of induced-pluripotent stem cell lines of early-onset PD distributed by Cedars Sinai. L.H.S. is on the Scientific Advisory Board of Lucy Therapeutics. D.G.S. is a member of the faculty of the University of Alabama at Birmingham and is supported by endowment and University funds. Dr. Standaert is an investigator in studies funded by Abbvie, Inc., the American Parkinson Disease Association, the Michael J. Fox Foundation for Parkinson Research, The National Parkinson Foundation, Alabama Department of Commerce, Alabama Innovation Fund, Genetech, the Department of Defense, and the NIH. He has a clinical practice and is compensated for these activities through the University of Alabama Health Services Foundation. He serves as Deputy Editor for the journal *Movement Disorders* and is compensated for this role by the International Parkinson and Movement Disorders Society. He has served as a consultant for or received honoraria from Abbvie Inc., Alnylam Pharmaceuticals, Appello, Biohaven Pharmaceuticals, Inc., BlueRock Therapeutics, Coave Therapeutics Curium Pharma, F. Hoffman-La Roche, Eli Lilly USA, Sanofi-Aventis, and Theravance, Inc. He has also received book royalties from McGraw-Hill Publishers. T.A.Y. has active grants from the American Parkinson

Disease Association, Travers Therapeutics, and the NIH (RF1NS115767-A1, R01NS112203, P50NS108675, U01NS104326, R13GM109532, T32GM008361). T.A.Y. serves on the Scientific Advisory Board for Parkinson's Foundation. TAY has received honorarium for presentations and panels from the Movement Disorders Society and for grant reviews from NIH. She has a U.S. Patent #7,919,262 on the use of 14-3-3s in neurodegeneration.

Author details

¹Duke Center for Neurodegeneration and Neurotherapeutics, Duke University, Durham, NC, USA

²Department of Pharmacology and Cancer Biology, Duke University, Durham, NC, USA

³Department of Neurology, University of Alabama at Birmingham, Birmingham, AL, USA

⁴Department of Neurodegenerative Science, Van Andel Institute, Grand Rapids, MI, USA

⁵Department of Neurology, Duke University, Durham, NC, USA

⁶Department of Pathology, Duke University, Durham, NC, USA

⁷Department of Neurobiology, Duke University, Durham, NC, USA

Received: 22 February 2024 / Accepted: 2 June 2024

Published online: 11 June 2024

References

1. Wszolek ZK, Pfeiffer B, Fulgham JR, Parisi JE, Thompson BM, Uitti RJ, et al. Western Nebraska family (family D) with autosomal dominant parkinsonism. *Neurology*. 1995;45:502–5.
2. Saunders-Pullman R, Mirelman A, Alcalay RN, Wang C, Ortega RA, Raymond D, et al. Progression in the LRRK2-Associated Parkinson Disease Population. *JAMA Neurol*. 2018;75:312–9.
3. Lake J, Reed X, Langston RG, Nalls MA, Gan-Or Z, Cookson MR, et al. Coding and noncoding variation in LRRK2 and Parkinson's Disease Risk. *Mov Disord*. 2022;37:95–105.
4. Bryant N, Malpeli N, Ziaee J, Blauwendraat C, Liu Z, AMP PD, Consortium, et al. Identification of LRRK2 missense variants in the accelerating medicines partnership Parkinson's disease cohort. *Hum Mol Genet*. 2021;30:454–66.
5. West AB, Schwarzschild MA. LRRK2-Targeting therapies March through the Valley of Death. *Mov Disord*. 2023. p. 361–5.
6. Steger M, Diez F, Dhakne HS, Lis P, Nirujogi RS, Karayel O et al. Systematic proteomic analysis of LRRK2-mediated Rab GTPase phosphorylation establishes a connection to ciliogenesis. *Elife* [Internet]. 2017;6. <https://doi.org/10.7554/eLife.31012>.
7. Liu Z, Xu E, Zhao HT, Cole T, West AB. LRRK2 and Rab10 coordinate macropinocytosis to mediate immunological responses in phagocytes. *EMBO J*. 2020;39:e104862.
8. Babbey CM, Ahktar N, Wang E, Chen CC-H, Grant BD, Dunn KW. Rab10 regulates membrane transport through early endosomes of polarized Madin-Darby canine kidney cells. *Mol Biol Cell*. 2006;17:3156–75.
9. Cardoso CMP, Jordao L, Vieira OV. Rab10 regulates phagosome maturation and its overexpression rescues Mycobacterium-containing phagosomes maturation. *Traffic*. 2010;11:221–35.
10. Gutierrez MG. Functional role(s) of phagosomal rab GTPases. *Small GTPases*. 2013;4:148–58.
11. Herbst S, Gutierrez MG. LRRK2 in infection: friend or foe? *ACS Infect Dis*. 2019;5:809–15.
12. Xu E, Boddu R, Abdelmotilib HA, Sokratian A, Kelly K, Liu Z, et al. Pathological α -synuclein recruits LRRK2 expressing pro-inflammatory monocytes to the brain. *Mol Neurodegener*. 2022;17:7.
13. Fraser KB, Moehle MS, Alcalay RN, West AB, LRRK2 Cohort Consortium. Urinary LRRK2 phosphorylation predicts parkinsonian phenotypes in G2019S LRRK2 carriers. *Neurology*. 2016;86:994–9.
14. Taymans J-M, Mutez E, Sibran W, Vandewynckel L, Deldycke C, Bleuse S, et al. Alterations in the LRRK2-Rab pathway in urinary extracellular vesicles as Parkinson's disease and pharmacodynamic biomarkers. *NPJ Parkinsons Dis*. 2023;9:21.
15. Sheng Z, Zhang S, Bustos D, Kleinheinz T, Le Pichon CE, Dominguez SL, et al. Ser1292 autophosphorylation is an indicator of LRRK2 kinase activity and contributes to the cellular effects of PD mutations. *Sci Transl Med*. 2012;4:164ra161.
16. Fan Y, Nirujogi RS, Garrido A, Ruiz-Martínez J, Bergareche-Yarza A, Mondragón-Rezola E, et al. R1441G but not G2019S mutation enhances LRRK2 mediated Rab10 phosphorylation in human peripheral blood neutrophils. *Acta Neuropathol*. 2021;142:475–94.
17. Liu Z, Bryant N, Kumaran R, Beilina A, Abeliovich A, Cookson MR, et al. LRRK2 phosphorylates membrane-bound Rabs and is activated by GTP-bound Rab7L1 to promote recruitment to the trans-golgi network. *Hum Mol Genet*. 2018;27:385–95.
18. Kozina E, Sadasivan S, Jiao Y, Dou Y, Ma Z, Tan H, et al. Mutant LRRK2 mediates peripheral and central immune responses leading to neurodegeneration in vivo. *Brain*. 2018;141:1753–69.
19. Biskup S, Moore DJ, Celsi F, Higashi S, West AB, Andrabi SA, et al. Localization of LRRK2 to membranous and vesicular structures in mammalian brain. *Ann Neurol*. 2006;60:557–69.
20. Alegre-Abarrategui J, Christian H, Lufino MMP, Muthiac R, Venda LL, Ansoorge O, et al. LRRK2 regulates autophagic activity and localizes to specific membrane microdomains in a novel human genomic reporter cellular model. *Hum Mol Genet*. 2009;18:4022–34.
21. Wang S, Unnithan S, Bryant N, Chang A, Rosenthal LS, Pantelyat A, et al. Elevated urinary Rab10 phosphorylation in idiopathic Parkinson Disease. *Mov Disord*. 2022;37:1454–64.
22. Black LL, Srivastava R, Schoeb TR, Moore RD, Barnes S, Kabarowski JH. Cholesterol-independent suppression of lymphocyte activation, autoimmunity, and Glomerulonephritis by Apolipoprotein A-1 in Normocholesterolemic Lupus-Prone mice. *J Immunol*. 2015;195:4685–98.
23. Hull TD, Kamal AI, Boddu R, Bolisetty S, Guo L, Tisher CC, et al. Heme Oxygenase-1 regulates myeloid cell trafficking in AKI. *J Am Soc Nephrol*. 2015;26:2139–51.
24. Boddu R, Hull TD, Bolisetty S, Hu X, Moehle MS, Daher JPL, et al. Leucine-rich repeat kinase 2 deficiency is protective in rhabdomyolysis-induced kidney injury. *Hum Mol Genet*. 2015;24:4078–93.
25. Starr ME, Steele AM, Saito M, Hacker BJ, Evers BM, Saito H. A new cecal slurry preparation protocol with improved long-term reproducibility for animal models of sepsis. *PLoS ONE*. 2014;9:e115705.
26. Fraser KB, Rawlins AB, Clark RG, Alcalay RN, Standaert DG, Liu N, et al. Ser(P)-1292 LRRK2 in urinary exosomes is elevated in idiopathic Parkinson's disease. *Mov Disord*. 2016;31:1543–50.
27. Käll L, Storey JD, Noble WS. Non-parametric estimation of posterior error probabilities associated with peptides identified by tandem mass spectrometry. *Bioinformatics*. 2008;24:42–8.
28. Nesvizhskii AI, Keller A, Kolker E, Aebersold R. A statistical model for identifying proteins by tandem mass spectrometry. *Anal Chem*. 2003;75:4646–58.
29. Zwiener I, Frisch B, Binder H. Transforming RNA-Seq data to improve the performance of prognostic gene signatures. *PLoS ONE*. 2014;9:e85150.
30. Benkert P, Meier S, Schaedelin S, Manouchehrinia A, Yaldizli Ö, Maceski A, et al. Serum neurofilament light chain for individual prognostication of disease activity in people with multiple sclerosis: a retrospective modelling and validation study. *Lancet Neurol*. 2022;21:246–57.
31. Davies P, Hinkle KM, Sukar NN, Sepulveda B, Mesias R, Serrano G, et al. Comprehensive characterization and optimization of anti-LRRK2 (leucine-rich repeat kinase 2) monoclonal antibodies. *Biochem J*. 2013;453:101–13.
32. Nirujogi RS, Tonelli F, Taylor M, Lis P, Zimprich A, Sammler E, et al. Development of a multiplexed targeted mass spectrometry assay for LRRK2-phosphorylated Rabs and Ser910/Ser935 biomarker sites. *Biochem J*. 2021;478:299–326.
33. Olah M, Menon V, Habib N, Taga MF, Ma Y, Yung CJ, et al. Single cell RNA sequencing of human microglia uncovers a subset associated with Alzheimer's disease. *Nat Commun*. 2020;11:6129.
34. Langston RG, Beilina A, Reed X, Kaganovich A, Singleton AB, Blauwendraat C, et al. Association of a common genetic variant with Parkinson's disease is mediated by microglia. *Sci Transl Med*. 2022;14:eabp8869.
35. Moehle MS, Webber PJ, Tse T, Sukar N, Standaert DG, DeSilva TM, et al. LRRK2 inhibition attenuates microglial inflammatory responses. *J Neurosci*. 2012;32:1602–11.
36. Gardet A, Benita Y, Li C, Sands BE, Ballester I, Stevens C, et al. LRRK2 is involved in the IFN-gamma response and host response to pathogens. *J Immunol*. 2010;185:5777–85.
37. Hakimi M, Selvanantham T, Swinton E, Padmore RF, Tong Y, Kabbach G, et al. Parkinson's disease-linked LRRK2 is expressed in circulating and tissue immune cells and upregulated following recognition of microbial structures. *J Neural Transm*. 2011;118:795–808.

38. Wang S, Kelly K, Brotchie JM, Koprich JB, West AB. Exosome markers of LRRK2 kinase inhibition. *NPJ Parkinsons Dis.* 2020;6:32.
39. Han Y, Bai X, Wang X. Exosomal myeloperoxidase as a biomarker of deep venous thrombosis. *Ann Transl Med.* 2022;10:9.
40. Peng L, Li X, Li Y, Zhao W, Nie S, Yu H, et al. Increased concentrations of myeloperoxidase in serum and serum extracellular vesicles are associated with type 2 diabetes mellitus. *Clin Chim Acta.* 2021;522:70–6.
41. Mir R, Tonelli F, Lis P, Macartney T, Polinski NK, Martinez TN, et al. The Parkinson's disease VPS35[D620N] mutation enhances LRRK2-mediated rab protein phosphorylation in mouse and human. *Biochem J.* 2018;475:1861–83.
42. Kuo Y-M, Li Z, Jiao Y, Gaborit N, Pani AK, Orrison BM, et al. Extensive enteric nervous system abnormalities in mice transgenic for artificial chromosomes containing Parkinson disease-associated alpha-synuclein gene mutations precede central nervous system changes. *Hum Mol Genet.* 2010;19:1633–50.
43. Sokratian A, Ziaee J, Kelly K, Chang A, Bryant N, Wang S, et al. Heterogeneity in α -synuclein fibril activity correlates to disease phenotypes in Lewy body dementia. *Acta Neuropathol.* 2021;141:547–64.
44. Wang X, Negrou E, Maloney MT, Bondar VV, Andrews SV, Montalban M, et al. Understanding LRRK2 kinase activity in preclinical models and human subjects through quantitative analysis of LRRK2 and pT73 Rab10. *Sci Rep.* 2021;11:12900.
45. Kelly K, Wang S, Boddu R, Liu Z, Moukha-Chafiq O, Augelli-Szafran C, et al. The G2019S mutation in LRRK2 imparts resiliency to kinase inhibition. *Exp Neurol.* 2018;309:1–13.
46. Holden SK, Finseth T, Sillau SH, Berman BD. Progression of MDS-UPDRS scores over five years in De Novo Parkinson Disease from the Parkinson's progression markers Initiative Cohort. *Mov Disord Clin Pract.* 2018;5:47–53.
47. Wissemann WT, Hill-Burns EM, Zabetian CP, Factor SA, Patsopoulos N, Hoggund B, et al. Association of Parkinson disease with structural and regulatory variants in the HLA region. *Am J Hum Genet.* 2013;93:984–93.
48. Matsumoto A, Takahashi Y, Chang H-Y, Wu Y-W, Yamamoto A, Ishihama Y, et al. Blood concentrations of small extracellular vesicles are determined by a balance between abundant secretion and rapid clearance. *J Extracell Vesicles.* 2020;9:1696517.
49. Jennings D, Huntwork-Rodriguez S, Henry AG, Sasaki JC, Meisner R, Diaz D, et al. Preclinical and clinical evaluation of the LRRK2 inhibitor DNL201 for Parkinson's disease. *Sci Transl Med.* 2022;14:eabj2658.
50. Jennings D, Huntwork-Rodriguez S, Vissers MFJM, Daryani VM, Diaz D, Goo MS, et al. LRRK2 inhibition by BLIB122 in healthy participants and patients with Parkinson's Disease. *Mov Disord.* 2023;38:386–98.
51. Wallings RL, Herrick MK, Tansey MG. LRRK2 at the Interface between Peripheral and Central Immune function in Parkinson's. *Front Neurosci.* 2020;14:443.
52. Garrido A, Fairfoul G, Tolosa ES, Marti MJ, Green A, Barcelona LRRK2 Study Group. α -synuclein RT-QuIC in cerebrospinal fluid of LRRK2-linked Parkinson's disease. *Ann Clin Transl Neurol.* 2019;6:1024–32.
53. Garrido A, Fairfoul G, Tolosa E, Marti MJ, Ezquerro M, Green AJE. Brain and cerebrospinal fluid α -Synuclein Real-Time Quaking-Induced Conversion identifies Lewy Body Pathology in LRRK2-PD. *Mov Disord.* 2023;38:333–8.
54. Merchant KM, Simuni T, Fedler J, Caspell-Garcia C, Brumm M, Nudelman KNH, et al. LRRK2 and GBA1 variant carriers have higher urinary bis(monacylglycerol) phosphate concentrations in PPMI cohorts. *NPJ Parkinsons Dis.* 2023;9:30.
55. Showalter MR, Berg AL, Nagourney A, Heil H, Carraway KL 3rd, Fiehn O. The Emerging and Diverse Roles of Bis(monoacylglycerol) Phosphate Lipids in Cellular Physiology and Disease. *Int J Mol Sci [Internet].* 2020;21. <https://doi.org/10.3390/ijms21218067>.
56. Mabrouk OS, Chen S, Edwards AL, Yang M, Hirst WD, Graham DL. Quantitative measurements of LRRK2 in human cerebrospinal fluid demonstrate increased levels in G2019S patients. *Front Neurosci.* 2020;14:526.
57. Gaetani L, Blennow K, Calabresi P, Di Filippo M, Parnetti L, Zetterberg H. Neurofilament light chain as a biomarker in neurological disorders. *J Neurosurg Psychiatry.* 2019;90:870–81.
58. Mielke MM, Hagen CE, Xu J, Chai X, Vemuri P, Lowe VJ, et al. Plasma phospho-tau181 increases with Alzheimer's disease clinical severity and is associated with tau- and amyloid-positron emission tomography. *Alzheimers Dement.* 2018;14:989–97.
59. Jiang C, Hopfner F, Berg D, Hu MT, Pilotto A, Borroni B, et al. Validation of α -Synuclein in L1CAM-Immunocaptured exosomes as a biomarker for the stratification of parkinsonian syndromes. *Mov Disord.* 2021;36:2663–9.
60. Okuzumi A, Hatano T, Matsumoto G, Nojiri S, Ueno S-I, Imamichi-Tatano Y, et al. Propagative α -synuclein seeds as serum biomarkers for synucleinopathies. *Nat Med.* 2023;29:1448–55.

Publisher's Note

Springer Nature remains neutral with regard to jurisdictional claims in published maps and institutional affiliations.